Vitamin B_{12} Conjugation of Peptide-$YY_{3–36}$ Decreases Food Intake Compared to Native Peptide-$YY_{3–36}$ Upon Subcutaneous Administration in Male Rats

Kelly E. Henry,* Clinton T. Elfers,* Rachael M. Burke, Oleg G. Chepurny, George G. Holz, James E. Blevins, Christian L. Roth, and Robert P. Doyle

Department of Chemistry (K.E.H., R.M.B., R.P.D.), Center for Science and Technology, Syracuse University, Syracuse, New York 13244; Center for Integrative Brain Research (C.T.E., C.L.R.), Division of Endocrinology, Seattle Children's Research Institute, Seattle, Washington 98101; Departments of Medicine (O.G.C., G.G.H., R.P.D.) and Pharmacology (G.G.H.), State University of New York, Upstate Medical University, Syracuse, New York 13210; Research and Development Service (J.E.B.), Veterans Affairs Puget Sound Health Care System, Seattle, Washington 98108; Department of Medicine (J.E.B.), Division of Metabolism, Endocrinology, and Nutrition, University of Washington, Seattle, Washington 98195; and Division of Endocrinology (C.L.R.), Department of Pediatrics, University of Washington, Seattle, Washington 98105

Challenges to peptide-based therapies include rapid clearance, ready degradation by hydrolysis/proteolysis, and poor intestinal uptake and/or a need for blood brain barrier transport. This work evaluates the efficacy of conjugation of vitamin B_{12} (B_{12}) on sc administered peptide tyrosine tyrosine $(PYY)_{3–36}$ function. In the current experiments, a B_{12}-$PYY_{3–36}$ conjugate was tested against native $PYY_{3–36}$, and an inactive conjugate B_{12}-PYY_{C36} (null control) in vitro and in vivo. In vitro experiments demonstrated similar agonism for the neuropeptide Y2 receptor by the B_{12}-$PYY_{3–36}$ conjugate (EC_{50} 26.5 nM) compared with native $PYY_{3–36}$ (EC_{50} 16.0 nM), with the null control having an EC_{50} of 1.8 μM. In vivo experiments were performed in young adult male Sprague Dawley rats (9 wk). Daily treatments were delivered sc in five 1-hour pulses, each pulse delivering 5–10 nmol/kg, by implanted microinfusion pumps. Increases in hindbrain Fos expression were comparable 90 minutes after B_{12}-$PYY_{3–36}$ or $PYY_{3–36}$ injection relative to saline or B_{12}-PYY_{C36}. Food intake was reduced during a 5-day treatment for both B_{12}-$PYY_{3–36}$- (24%, $P = .001$) and $PYY_{3–36}$-(13%, $P = .008$) treated groups relative to baseline. In addition, reduction of food intake after the three dark cycle treatment pulses was more consistent with B_{12}-$PYY_{3–36}$ treatment (−26%, −29%, −27%) compared with the $PYY_{3–36}$ treatment (−3%, −21%, −16%), and B_{12}-$PYY_{3–36}$ generated a significantly longer inhibition of food intake vs $PYY_{3–36}$ treatment after the first two pulses ($P = .041$ and $P = .036$, respectively). These findings demonstrate a stronger, more consistent, and longer inhibition of food intake after the pulses of B_{12}-$PYY_{3–36}$ conjugate compared with the native $PYY_{3–36}$. **(*Endocrinology* 156: 1739–1749, 2015)**

Peptide tyrosine tyrosine (PYY), along with neuropeptide Y (NPY) and pancreatic polypeptide (PP), is a member of PP-fold family and has been shown to have clinical relevance in appetite control and energy homeostasis (1). PYY is expressed in the enteroendocrine L cells of the large intestine and secreted in proportion to caloric intake (2) and exercise (3). Studies have shown that the truncated form of PYY, $PYY_{3–36}$, inhibits food intake in rodents (4–7), nonhuman primates (8, 9), and humans (3, 7, 10, 11). The anorectic effect of $PYY_{3–36}$ is due to the agonism of the NPY2 receptor located both in the intestines (vagal-brain afferent signaling) (4, 12) and the arcu-

ISSN Print 0013-7227 ISSN Online 1945-7170
Printed in U.S.A.

Received October 9, 2014. Accepted February 3, 2015.
First Published Online February 6, 2015

* K.E.H. and C.T.E. are co-first authors, and C.L.R. and R.P.D. are co-senior authors.

Abbreviations: AUC, area under the curve; B_{12}, vitamin B_{12}; BBB, blood-brain barrier; C_{max}, maximum plasma concentration; NPY, neuropeptide Y; NTS, nucleus of the solitary tract; PP, pancreatic polypeptide; PYY, peptide tyrosine tyrosine; TCII, transcobalamin II; V_D/F, volume of distribution.

ate nucleus of the hypothalamus (5, 7). $PYY_{3–36}$ also inhibits gastric emptying (13), which creates a prolonged feeling of fullness, contributing to the anorectic effects of the peptide. Obese individuals have reduced concentrations of $PYY_{3–36}$ in the fasted state and after a caloric load (14–16), but after weight loss and/or gastric bypass surgery, circulating concentrations of $PYY_{3–36}$ return to levels representative of average-weight individuals (14). This indicates that obesity does not result from resistance to PYY but from a lack of circulating peptide, making it attractive as a clinical drug target. The issue with $PYY_{3–36}$ development as a pharmaceutical lies in both the need to inject it and its relatively short half-life (~8 min) due to degradation by enzymes such as meprin-β (17). In addition, rapid increases in $PYY_{3–36}$ levels can lead to nausea (18) as well as peptide-induced malaise via high dosing in mice (19) and humans (20). Reports of PEGylation (21) and conjugation to albumin (22) have improved the half-life for $PYY_{3–36}$, but the PEG requires removal for function in vivo (21), and both have an inability to cross the blood-brain barrier (23). We have been interested in using the vitamin B_{12} (B_{12}) dietary uptake pathway for peptide delivery (herein specifically through conjugation of B_{12} to $PYY_{3–36}$) to prolong peptide activity and/or improve peptide delivery to the brain for obesity drug development.

Mammals (including humans and rats) have a highly efficient uptake and transport mechanism for the absorption and cellular uptake of B_{12} (24). To successfully use the dietary uptake pathway of B_{12}, recognition and affinity for the B_{12} binding proteins must not be lost or diminished via conjugation to the target peptide, nor can the peptide function be lost due to conjugation to B_{12}. Literature has shown that the conjugation to the 5′ hydroxyl group of the ribose ring on B_{12} does not affect recognition of B_{12} by carrier proteins such as haptocorrin (located in saliva, stomach, and upper duodenum), intrinsic factor (located in stomach and upper and lower intestines), or transcobalamin II (TCII; located in serum) (25, 26). Doyle and colleagues have established the coupling of peptides such as insulin (27), $PYY_{3–36}$ (28), and glucagon-like peptide-1 (29) to B_{12} using 1,1′-carbonyl-(1, 2, 4)-triazole coupling chemistry.

Although $PYY_{3–36}$ has been confirmed to cross the blood-brain barrier (BBB) via nonsaturable mechanisms (30), B_{12} can also cross the BBB, likely via a process facilitated by the serum B_{12} binding protein TCII (31). Doyle et al (28) recently demonstrated that a clinically relevant level (>180 pg/mL) of $PYY_{3–36}$ could be delivered orally in rats via conjugation to vitamin B_{12}. However, to date, no feeding studies exist that test these compounds for function in vivo. In addition, questions as to whether conjugation of B_{12} to $PYY_{3–36}$ would affect, negatively or positively, the function of $PYY_{3–36}$ in vitro and/or in vivo remain unanswered.

The goal of this work was to evaluate the effects of conjugation of B_{12} on $PYY_{3–36}$ function in vitro and in vivo by sc administration to ultimately use the B_{12} dietary pathway for $PYY_{3–36}$ clinical use. The results observed indicate that conjugation with B_{12} has little effect on $PYY_{3–36}$ function in vitro with comparable agonism of the NPY2 receptor with both B_{12}-$PYY_{3–36}$ and native $PYY_{3–36}$. However, in vivo pharmacodynamics studies demonstrate stronger reduction of food intake and weight gain for B_{12}-$PYY_{3–36}$ relative to $PYY_{3–36}$ pulses, concomitant with increased plasma half-life, slower clearance, and greater tissue distribution.

Materials and Methods

All syntheses and purification methods, along with all chemicals, solvents, and reagents used, are described in the Supplemental Materials along with analytical data and liquid chromatograms (see Supplemental Figures 1–5).

In vitro determination of NPY2-receptor agonism via calcium mobilization assay (fura-2)

Chinese hamster ovary-K1 cells were plated in a 96-well plate at a density of 20 000 cells/well on rat tail collagen-coated black Costar 3904 plates and incubated overnight at 37°C and 5% CO_2. The next day, the cells were transfected with NPY2R and GαqG66Di5 (32) using Lipofectamine 2000 (Life Technologies) according to the manufacturer's instructions. The cells were cultured in F-12K containing 10% fetal bovine serum for 48 hours. After transfection, the cells were loaded with fura-2 (1 μM Fura-2AM) in a standard extracellular solution containing 138 mM NaCl, 5.6 mM KCl, 2.6 mM $CaCl_2$, 1.2 mM $MgCl_2$, 10 mM HEPES (pH 7.4), and 11.1 mM glucose, additionally supplemented with 20 μL/mL of fetal bovine serum and 1 μL/mL of Pluronic F-127. Spectrofluorimetry was performed using excitation light at 355/9 and 375/9 nm (center/band pass) delivered using a 455-nm dichroic mirror. Emitted light was detected at 505/15 nm, and the ratio of emission light intensities due to excitation at 355 and 375 nm was calculated.

Animal experiments

All procedures were conducted in accordance with the National Institutes of Health Guide for the Care and Use of Laboratory Animals and were approved by the Seattle Children's Research Institute Institutional Animal Care and Use Committee. Nine-week-old male Sprague Dawley rats (300–330 g, CD-IGS; Charles River Labs) were acclimated for 14 days to a 12-hour light, 12-hour dark cycle, with lights on at 9:00 PM and lights off at 9:00 AM. The rats were well handled throughout the acclimation phase to accustom them to the researchers and minimize any induced stress through the later phases of the experiment. The source of diet was ad libitum standard chow diet (5053 PicoLab Rodent Diet 20; LabDiet) ground to a fine powder. Rats had ad libitum access to water. Food intake was continuously recorded

using AccuScan DietMax (currently OmniTech Electronics, Inc Diet System) cages for a 22.5-hour period each day. Access to food was withheld during the 1.5-hour period just prior to the start of the dark cycle for cage maintenance and daily measurement of body weight. All food intake data were binned into 15-minute intervals for analysis. All peptides were dissolved in sterile saline (0.9% sodium chloride injection, USP) prior to administration.

In vivo dose response of sc administered B_{12}-$PYY_{3–36}$ on 3-hour food intake in rats

Food intake was recorded for 2 days before and 3 days after the 5-day treatment phase for the establishment of normal intake. During the 5-day treatment phase, three B_{12}-$PYY_{3–36}$ treatments (3, 5, and 10 nmol/kg; one per day) were administered to the rats (n = 5) 15 minutes prior to the start of the dark cycle via an sc injection with one washout day in between administrations.

B_{12}-$PYY_{3–36}$, $PYY_{3–36}$, or B_{12}-PYY_{C36} sc pulsatile infusion on food intake

The study consisted of a 5-day baseline phase, a 5- or 10-day treatment phase, and a 5-day compensation phase. Sterile saline-filled iPrecio microinfusion pumps (Primetech Corp) were surgically implanted into the sc space on the dorsal side of the animal posterior to the left scapula and anchored to the muscle wall with silk suture. From the implanted pump, a catheter was tunneled to a small sc pocket on the dorsal side of the neck in which it was anchored in place. Animals were given a 7-day recovery period before beginning the baseline phase of the study. During both the recovery and baseline phases of the experiment, the patency of the catheter was maintained by a steady saline infusion at a rate of 2 μL/h. The pump reservoir was refilled with sterile injectable saline as necessary. Patency was verified by the volume removed during exchange of pump contents and the volume remaining at the end of the experiment.

At the start of the treatment phase, the remaining saline was removed from the pump and the reservoir was filled with the assigned drug ($PYY_{3–36}$, n = 8; B_{12}-$PYY_{3–36}$, n = 9; or B_{12}-PYY_{C36}, n = 5). The microinfusion pumps were preprogrammed to prime the catheter after the content change and to shut off at the end of the treatment phase. Due to a set infusion cycle, all drug doses were based on body weight at the beginning of the treatment phase. Treatments were delivered sc with five pulses per day; three 1-hour pulses of 10 nmol/kg/h (20 μL/h) starting 15 minutes prior to lights out with 3 hours between pulses and 2 1-hour pulses of 5 nmol/kg/h (10 μL/h) starting 15 minutes prior to lights on with 5 hours between pulses. Between all pulses a basal infusion rate of 0.5 nmol/kg/h (1 μL/h) was used to maintain patency. After the end of the treatment phase, the animals were observed for an additional 5 days to monitor for compensation of food intake in defense of their normal body weight gain.

Investigating the effect of sc administered B_{12}-$PYY_{3–36}$ and B_{12}-PYY_{C36} in Fos activation in the hindbrain relative to $PYY_{3–36}$ and saline

After a 4-hour fast, rats (n = 3–5/group) were given a sc injection of saline, B_{12}-PYY_{C36} (10 nmol/kg; null control), B_{12}-$PYY_{3–36}$ (10 nmol/kg), or $PYY_{3–36}$ (10 nmol/kg) and deeply anesthetized 90 minutes later with an overdose of isoflurane. Five minutes later, animals were transcardially perfused with 4% paraformaldehyde in 0.1 M PBS (pH 7.4). Brains were removed, stored overnight in fresh fixative at 4°C and subsequently transferred to 0.1 M PBS containing 25% sucrose for 48 hours and then frozen in isopentane at −80°C and stored at −80°C. Coronal 14-μm cryostat sections were thaw mounted onto slides and stored at −30°C.

Immunohistochemistry with antisera to c-Fos was performed on anatomically matched sections throughout the nucleus of the solitary tract (NTS) with tissue from every treatment condition included in every batch. For full details, see the Supplemental Materials.

In vivo uptake studies

$PYY_{3–36}$ (n = 3) and B_{12}-$PYY_{3–36}$ conjugate (n = 4) were administered via sc injection at a dose of 10 nmol/kg. Blood samples were retrieved via tail tip snip at 0, 15, 30, 60, 90, 120, 180, 240, and 300 minutes using potassium EDTA-coated microvettes (Microvette 100 K3E) pretreated with dipeptidyl peptidase-IV inhibitor (EMD Millipore). After the collection, blood samples were immediately placed on ice and then centrifuged at 3000 × *g* for 15 minutes at 4°C. Plasma samples were kept on dry ice or stored in a −80°C freezer until assayed. Human $PYY_{3–36}$ was quantified by enzyme immunoassay (EIA) via EZHPYYT66K human PYY (total) ELISA kit (EMD Millipore).

Statistics

All results are expressed as mean ± SEM. Statistical analyses were performed using GraphPad Prism Software. For unadjusted analyses, a one-way ANOVA with Tukey's multiple comparison test post hoc test was used to compare mean values between multiple groups, and a two-sample unpaired Student's *t* test was used for two-group comparisons. Paired *t* tests (two tailed) were used to detect the differences in measures between phases within the treatment groupings. In all instances, a value of $P < .05$ was considered significant.

Results

PYY structure and conjugate synthesis

$PYY_{3–36}$ demonstrates significant tertiary structure for such a small peptide (Figure 1A). The C-terminal pentapeptide region (orange) is critical for association with the NPY2 receptor (33). Molecular dynamics simulation of B_{12}-$PYY_{3–36}$ shows how the B_{12} and $PYY_{3–36}$ interact in space (Figure 1B). B_{12}-amino butyne (B_{12}-AB) was conjugated to $PYY_{3–36}$ modified at the K4 lysine position to an azide via its alkyne tail, forming a 1,2,3-triazole linkage via Cu(I)-mediated Sharpless/Huisgen (34) click chemistry (Figure 1C).

In vitro characterization of conjugates via fura-2 assay at the NPY1 and NPY2 receptors

Comparable activity of B_{12}-$PYY_{3–36}$ conjugate produced by coupling of the vitamin ribose moiety to $PYY_{3–36}$ K4 lysine(EC_{50} 26.51 nM) to native $PYY_{3–36}$ (EC_{50} 16.07 nM) was measured via calcium mobilization assay via the

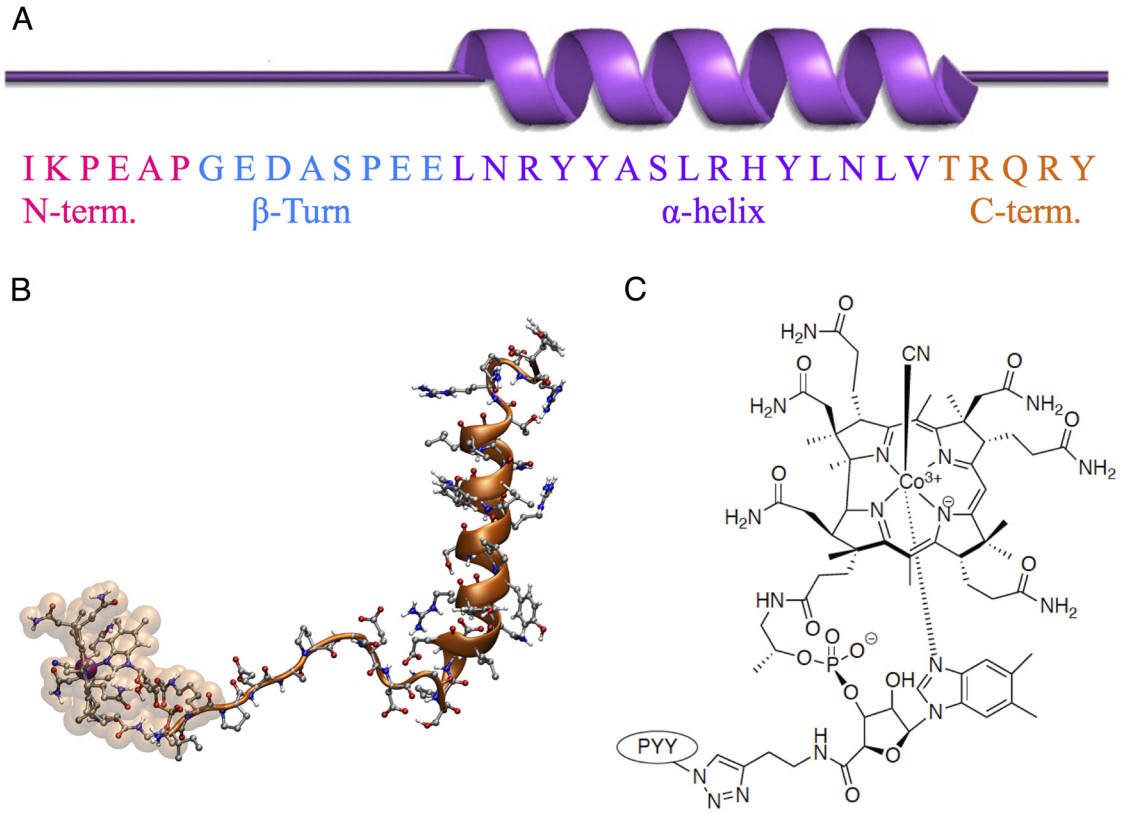

Figure 1. Secondary structure of PYY (A) and how the PYY N terminus is connected to vitamin B_{12} by molecular dynamics (B) and a more detailed look at the triazole linkage between PYY K4-azide modified and B_{12}-amino butyne (C).

NPY2 receptor cascade in transfected Chinese hamster ovary-K1 cells cotransfected with GαqG66Di5 (32). A null conjugate obtained by the conjugation of B_{12} at the C terminus of $PYY_{3–36}$ (EC_{50} 1.809 μM) was also produced as a control (Figure 2A). Agonism of the NPY1 receptor was confirmed with $PYY_{1–36}$ (EC_{50} 9.794 nM) as the native ligand control for this receptor. NPY1 activity was significantly reduced for $PYY_{3–36}$ (EC_{50} 619.6 nM) and B_{12}-$PYY_{3–36}$ (EC_{50} 2.2 μM) (Figure 2B).

Effect of B_{12}-$PYY_{3–36}$ on 3-hour food intake and in vivo uptake profile over 5 hours

Subcutaneous administration of 10 nmol/kg B_{12}-$PYY_{3–36}$ was the only dose to produce an immediate response, attenuating rate of food intake for approximately 45 minutes starting 30 minutes after the injection. Additionally, the 10-nmol/kg dose produced a significant reduction of food intake 3 hours after the injection (P = .047); lower doses failed to yield any significant changes compared with baseline (3 nmol/kg, P = .954; 5 nmol/kg, P = .966) (Figure 3A).

Subsequent uptake studies were then performed at the 10 nmol/kg dose for both $PYY_{3–36}$ and B_{12}-$PYY_{3–36}$ (Figure 3B). The calculated, extrapolated area under the curve (AUC) value (AUC_{ext}) is significantly higher (~1.8-fold) for B_{12}-$PYY_{3–36}$ (7130 ± 2050 pg/h/mL) than $PYY_{3–36}$ (3843 ± 1125 pg/h/mL), suggesting the extent of sc absorption is greater for B_{12}-$PYY_{3–36}$ (maximum plasma concentration (C_{max}) of 2520 ± 257 pg/mL) than $PYY_{3–36}$ (C_{max} of 1680 ± 243 pg/mL). The rate of absorption, however, was noted to be similar with time to C_{max} of 0.63 hours for B_{12}-$PYY_{3–36}$ and 0.58 hours for $PYY_{3–36}$; a result supported by the fact that both $PYY_{3–36}$ and B_{12}-$PYY_{3–36}$ have the same time to nadir of pulse (vide infra; see Figure 6A). Further comparison of primary pharmacokinetic parameters showed positive effects of B_{12} conjuga-

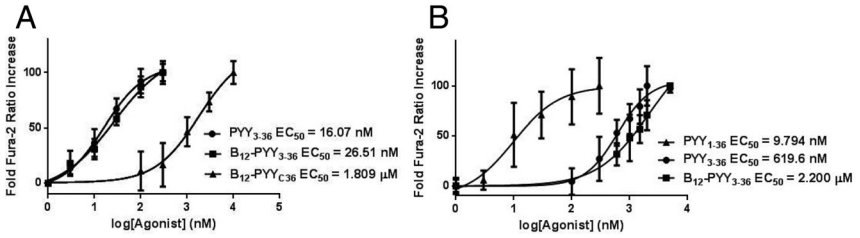

Figure 2. A, Dose-response curves of $PYY_{3–36}$, B_{12}-$PYY_{3–36}$, and B_{12}-PYY_{C36} null control with respective EC_{50} values as determined by fura-2 activity at the NPY2 receptor. B, Dose-response curves of $PYY_{1–36}$ (run as an internal control), $PYY_{3–36}$, and B_{12}-$PYY_{3–36}$ with respective EC_{50} values were determined by fura-2 activity at the NPY1 receptor.

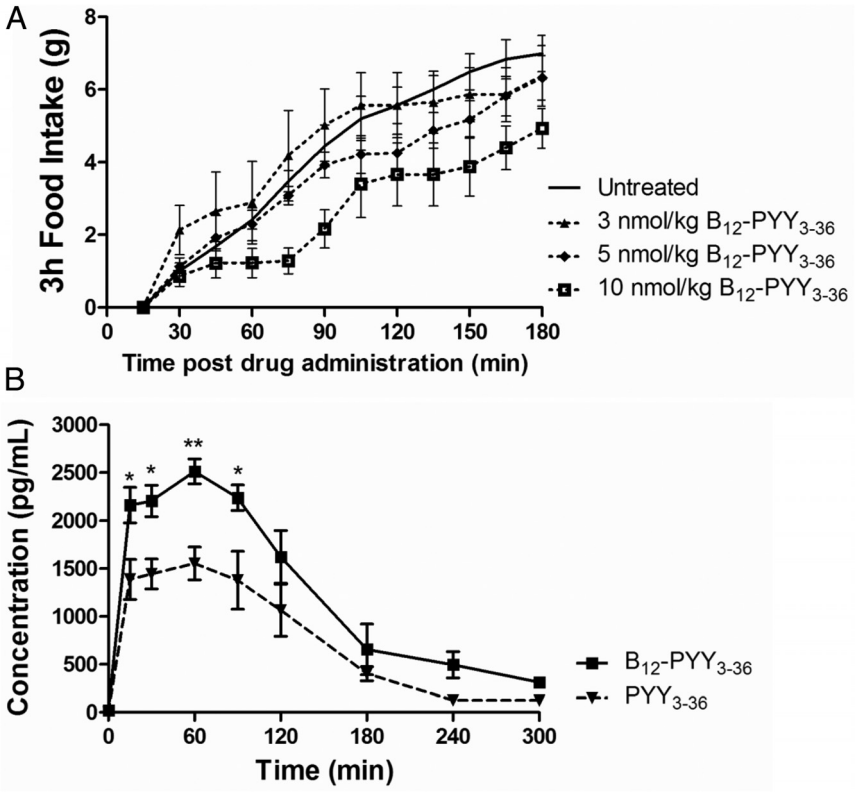

Figure 3. A, Dose response to sc injected B_{12}-$PYY_{3–36}$ on cumulative food intake in five rats, demonstrating only 10 nmol/kg, produced a rapid and prolonged FI reduction. B, Pharmacokinetic profile of B_{12}-$PYY_{3–36}$ (n = 4) and $PYY_{3–36}$ (n = 3) sc injected at 10 nmol/kg. *, $P < .05$; **, $P < .01$ compared with $PYY_{3–36}$.

tion on both volume of distribution (V_D/F; 15.0 ± 1.5 L/kg for B_{12}-$PYY_{3–36}$ vs 12.8 ± 1.5 L/kg for $PYY_{3–36}$) and clearance (133 ± 32 mL/min/kg for B_{12}-$PYY_{3–36}$ vs 188.6 ± 65.5 mL/min/kg for $PYY_{3–36}$). The ratio of V_D/F to clearance was 1:14.7 for $PYY_{3–36}$ and 1:8.9 for B_{12}-$PYY_{3–36}$, a change reflected in the observed half-lives of both (0.82 ± 0.16 h vs 1.34 ± 0.28 h, respectively).

Effect of B_{12}-$PYY_{3–36}$ on food intake

All analyses for 5-day treatment effects contain measurements from all animals. Prior to treatment, average baseline food intake profile (Figure 4A) was established using data collected over 5 days from all 22 rats ($PYY_{3–36}$, n = 8; B_{12}-$PYY_{3–36}$, n = 9; or B_{12}-PYY_{C36}, n = 5). A sixth order smoothing polynomial averaging over the four neighboring values on either side was fit to the collective baseline data and actual SEM values were applied to the smoothed curve. Results show a pattern with a distinct peak at both ends of dark cycle with a relatively steady food intake in between (Figure 4A). No significant differences in cumulative food intake were observed between groups for the 5-day baseline phase ($P = .377$). Representative average daily food intake patterns of single animals from each treatment group during the 5-day treatment compared with the baseline conditions are shown and illustrate an altered pattern of food intake from $PYY_{3–36}$ (Figure 4B), stronger reduction of food intake from B_{12}-$PYY_{3–36}$ with essentially no peaks above the baseline profile (Figure 4C), and no significant effect on food intake with B_{12}-PYY_{C36} (Figure 4D). The averaged food intake for all animals per group over the 5-day period showed more pronounced reductions and longer durations of reduced food intake in B_{12}-$PYY_{3–36}$ conjugate (Figure 4E) vs $PYY_{3–36}$ treated animals (Figure 4F).

Analysis of cumulative food intake of all treated rats ($PYY_{3–36}$, n = 8; B_{12}-$PYY_{3–36}$, n = 9; or B_{12}-PYY_{C36}, n = 5) on treatment day 5 indicated an overall effect of treatment ($P = .029$), with a significant difference between the null control and B_{12}-$PYY_{3–36}$ groups; no other group comparisons were significant (Figure 5A). Compared with the baseline, the first 3 days of treatment produced the largest effect on food intake, specifically with B_{12}-$PYY_{3–36}$ treatment ($P = .002$), but also with $PYY_{3–36}$ ($P = .020$) treatment (Figure 5B). During days 4 and 5 of the treatment phase, the reductions of food intake were less severe, although they were still significant for the two treatment groups (B_{12}-$PYY_{3–36}$, $P = .006$; $PYY_{3–36}$, $P = .033$) (Figure 5B).

A subgroup of animals (B_{12}-$PYY_{3–36}$, n = 6; $PYY_{3–36}$, n = 4; B_{12}-PYY_{C36}, n = 4) received a longer (10 d) treatment to determine any changes in efficacy during prolonged treatment. Treatment days 6–10 yielded a comparable reduction in average daily food intake compared with days 4 and 5 (Figure 5, C and D, shows results for this subgroup). Both B_{12}-$PYY_{3–36}$ and $PYY_{3–36}$ treatment resulted in similar patterns of reduced cumulative food intake relative to baseline over the course of the 10-day treatment (Figure 5C), with maximal reductions occurring at day 3. Overall 10-day mean daily food intake was significantly lower than baseline for both treatment groups (B_{12}-$PYY_{3–36}$ 17.6 ± 1.0 vs 22.7 ± 0.2 g/d, $P = .002$; $PYY_{3–36}$ 19.3 ± 0.75 vs 23.7 ± 1.0 g/d, $P = .001$).

The effects of each pulse of treatment on the food intake pattern were analyzed, ie, time between start of drug pulse and nadir of reduced food intake as well as duration of reduced food intake after a pulse compared with baseline. Duration of reduced food intake was defined as the length

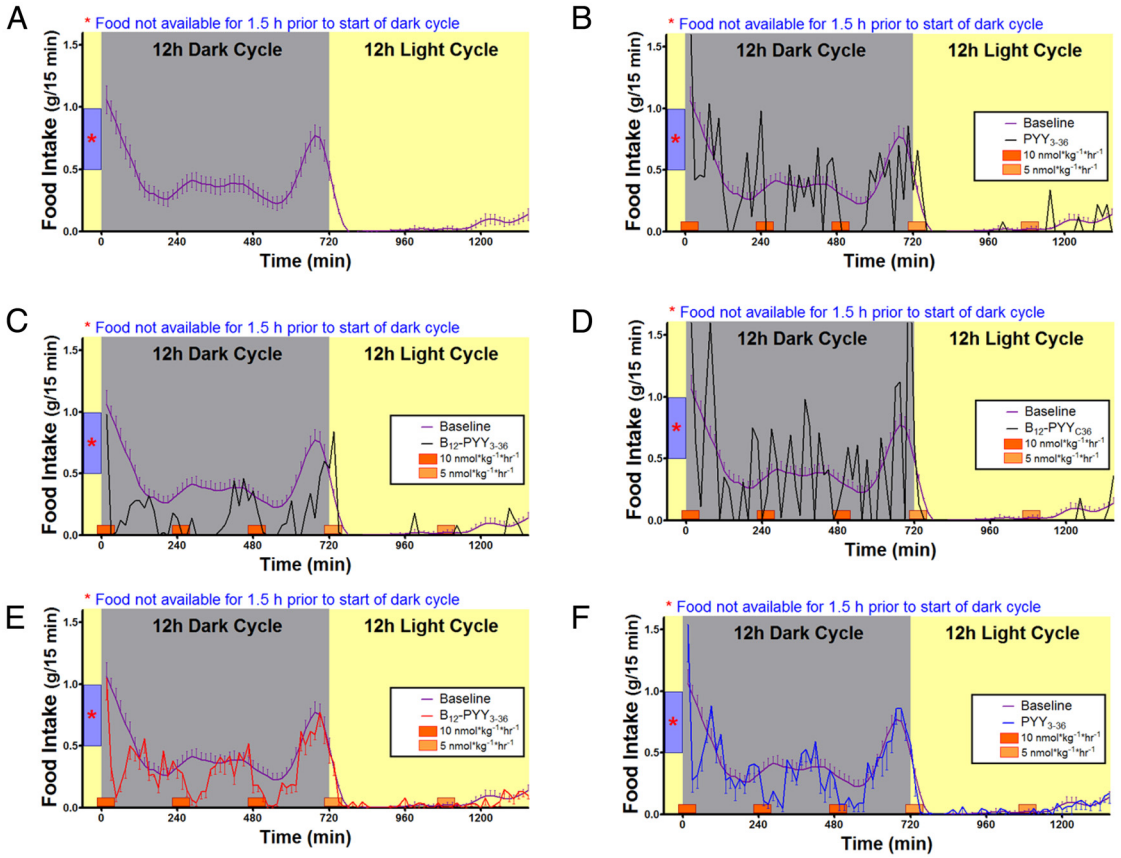

Figure 4. Twenty-four-hour food intake patterns averaged over 5 days' duration. Food intake under baseline conditions in 22 rats (A) in comparison with after treatments receiving pulses of B_{12}-$PYY_{3–36}$ conjugate (n = 9), $PYY_{3–36}$ (n = 8), or the null conjugate B_{12}-PYY_{C36} (n = 6). Representative food intake patterns of single animals receiving drugs $PYY_{3–36}$ (B), B_{12}-$PYY_{3–36}$ (C), or B_{12}-PYY_{C36} (D), respectively, are shown. The averaged food intake for all animals per group over 5 days are shown for rats treated by B_{12}-$PYY_{3–36}$ conjugate (E) vs $PYY_{3–36}$ (F).

of time after the start of each infusion pulse in which the 15-minute binned food intake remained lower than the average baseline food intake profile − 1 SEM and was calculated for the individual animals during the 5-day treatment phase. Results show that both drugs, B_{12}-$PYY_{3–36}$ and $PYY_{3–36}$, produced a maximum reduction in food intake compared with baseline at 41 minutes after the start of the first pulse during dark cycle (Figure 6A). However, the duration (Figure 6B) and magnitude (Figure 6C) of food intake reduction after the first pulse was significantly greater in B_{12}-$PYY_{3–36}$ compared with $PYY_{3–36}$. Administration of B_{12}-$PYY_{3–36}$ resulted in highly consistent reductions of food intake relative to baseline after all three-drug pulses during the dark cycle (one way ANOVA across three pulses $P = .976$), which was not observed for $PYY_{3–36}$ (one way ANOVA $P = .063$) (Figure 6D). The null control, B_{12}-PYY_{C36} yielded no significant changes in food intake compared with baseline.

Effect of B_{12}-$PYY_{3–36}$ on body weight gain

Prior to drug administration, body weights were comparable in animals of all treatment groups ($PYY_{3–36}$, 366.6 ± 10.0 g; B_{12}-$PYY_{3–36}$, 368.2 ± 6.6 g; B_{12}-PYY_{C36}, 370.4 ± 9.5 g, $P = .942$). A significant reduction in daily body weight gain was observed during the first 3 days of treatment in both groups (B_{12}-$PYY_{3–36}$, $P = .004$; $PYY_{3–36}$, $P = .003$) (Figure 7). However, reduction of body weight gain did not last beyond this time point in these lean animals.

Changes in Fos activation in the hindbrain

At the time the animals were killed, sc administration of $PYY_{3–36}$ and B_{12}-$PYY_{3–36}$ elicited nearly twice as many Fos (+) cells in the NTS relative to saline or B_{12}-PYY_{C36} (null control) injection ($P < .05$ for both comparisons active compounds vs null control, Figure 8A). No difference was observed in the number of Fos (+) cells detected between saline- or B_{12}-PYY_{C36}-treated controls or between either active compound (B_{12}-$PYY_{3–36}$ and $PYY_{3–36}$) (Figure 8B).

Discussion

$PYY_{3–36}$ is an attractive clinical drug target due to its anorectic effect and decreased circulation concentration in

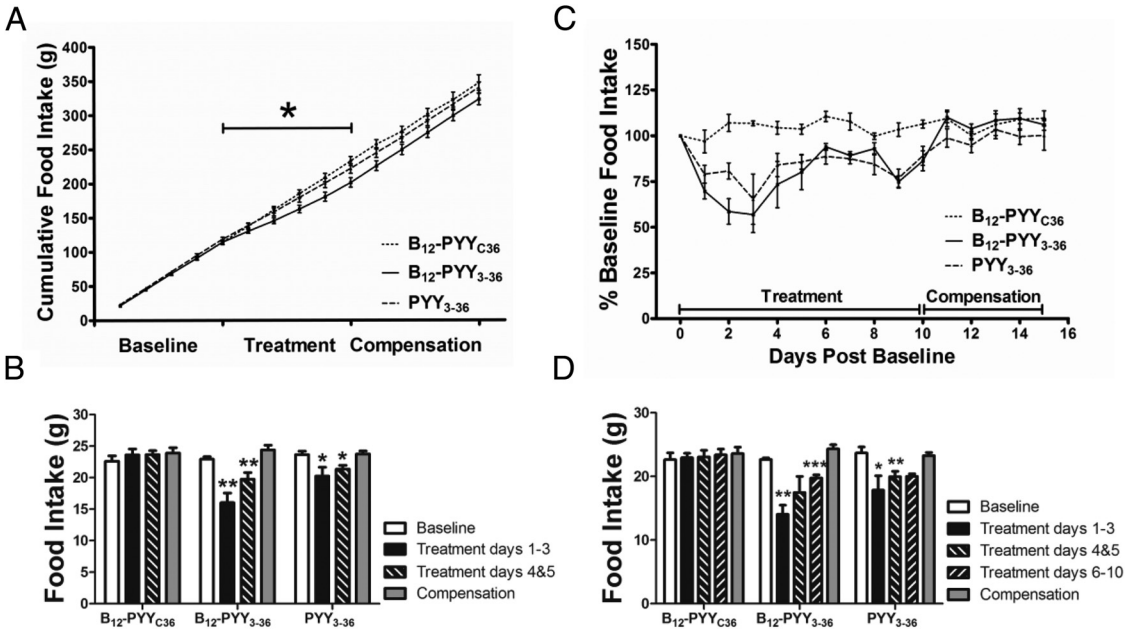

Figure 5. Daily food intake during baseline conditions, during 5-day drug administration, and after a compensation period displayed as cumulative food intake (A) and averaged daily food intake data comparing baseline and compensation period vs treatment days 1–3 and 4 and 5 of all treated animals (B). Percentage changes of food intake compared with baseline for a 10-day treatment (C) and averaged daily food intake data comparing baseline and compensation period vs treatment days 1–3, 4 and 5, and 6–10 of the 10-day treatment subgroup (D). *, $P < .05$; **, $P < .01$; ***, $P < .001$ compared with baseline.

obese individuals; however, its relatively short half-life and required method of delivery are limiting factors in its clinical application. Using B_{12} and associated binding proteins and uptake receptors is an interesting, possible solution to these limitations. The presented study shows that conjugation of B_{12} to $PYY_{3–36}$ at the peptide K4 position yielded a conjugate that is similar in bioactivity to the native peptide in vitro and results in improved absorption and reduction in food intake in vivo. The significance of this study lies in it showing, for the first time, that conjugation of a gut hormone to B_{12} not only exhibits comparable bioactivity but indeed imparts improved pharmacology.

In vitro testing of the B_{12}-$PYY_{3–36}$ conjugate demonstrated comparable agonism of the NPY2 receptor to $PYY_{3–36}$ as measured through fura-2 fluorescence via cytosolic calcium mobilization; both EC_{50} values are in the low nanomolar range. The B_{12}-PYY_{C36} null conjugate control was determined, as suspected, to have greatly diminished agonism at the NPY2 receptor, resulting in an EC_{50} in the low micromolar range, as shown in Figure 2A.

In vitro testing of $PYY_{3–36}$ and B_{12}-$PYY_{3–36}$ against the NPY1 receptor was also assayed to measure any potential difference in agonism between the conjugate and $PYY_{3–36}$. The NPY1 native substrate $PYY_{1–36}$ was used as the internal control (measured EC_{50} 9.8 nM). As expected, greatly diminished activity for NPY1R vs NPY2R was observed for $PYY_{3–36}$ (EC_{50} 619.6 nM) and B_{12}-$PYY_{3–36}$ (EC_{50} 2.2 μM), as shown in Figure 2B. This noted difference in NPY1 activity would be expected to play no significant role in the differences observed in function herein but again indicated the importance of the N terminus in selectivity for NPY1R over NPY2R.

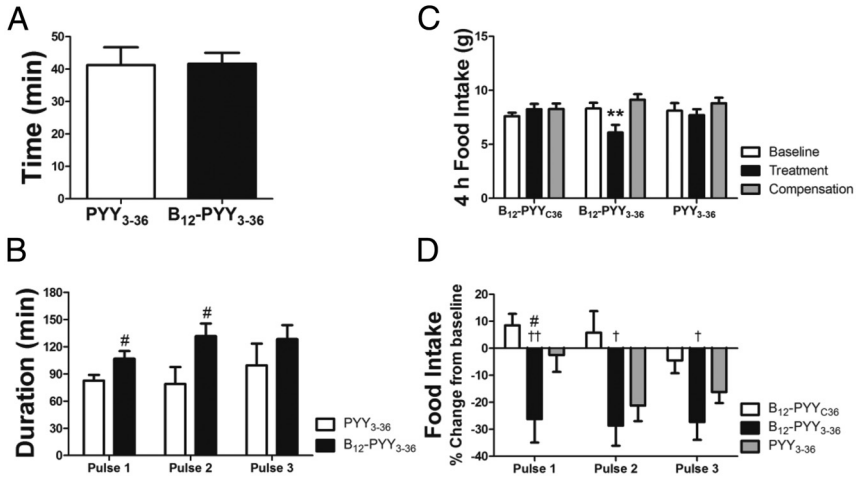

Figure 6. Analyses of food intake reduction in relation to drug pulses during 5-day treatment. Occurrence of food intake nadir after start of first drug pulse at dark cycle (A). Duration of reduced food intake after the three drug pulses (B) during the dark cycle. Food intake during the first 4 hours of the dark cycle (C) and relative changes of food intake after drug pulses 1–3 (D). #, $P < .05$ compared with $PYY_{3–36}$; †, $P < .05$; ††, $P < .01$ compared with B_{12}-PYY_{C36}.

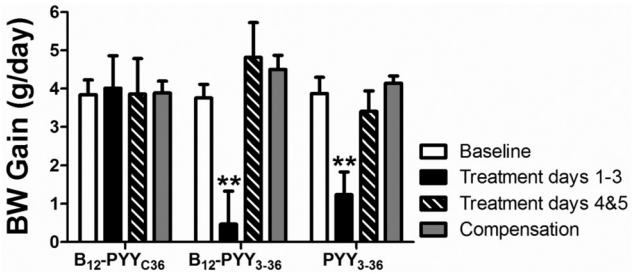

Figure 7. Effects on weight gain. Reduced body weight gain was observed during the first 3 days of treatment in both groups but not during treatment days 4 and 5. **, $P < .01$ compared with baseline.

In vivo testing of the B_{12}-$PYY_{3–36}$ conjugate centered on longitudinal and cross-sectional changes in food intake and body weight gain as well as Fos activation in the hindbrain after treatment. The approach used to represent the baseline food intake profile yields a generalized representation of the normal food intake pattern of a rat and provided a benchmark by which to assess duration of reduced food intake after drug administration pulses.

The treatment infusion profile was designed around the normal food intake pattern of rats during both the light and dark cycles. Specifically, three 1-hour pulses were used to deliver a full treatment just prior to the feeding peaks occurring at the start and end of the dark cycle as well as the plateau in the middle. The two half-doses were used to help prevent a compensation of food intake at the start of the light cycle just before the rats begin resting and halfway through the dark cycle when light feeding begins to occur. Likewise, the treatment dose was selected to produce a robust effect, with an interpulse period long enough to resume normal feeding prior to the next dose, thus allowing for a separation of treatment effects in each pulse period. The 10-nmol/kg dose was used because it was the only dose to show an immediate response, nearly halting food intake for a 45-minute period 30 minutes after the injection, whereas lower doses (3 and 5 nmol/kg) did not have this effect (Figure 3A). This sc administered dose of $PYY_{3–36}$ is consistent with dosing in previous experiments and is well below the 1000 μg/kg (247 nmol/kg) ip dose shown to produce no conditioned taste aversion (35) in rats. After this period, food intake resumed at a comparable rate with the untreated condition; however, 3 hours after the administration, the reduction of food intake was not compensated for, yielding a significant change in cumulative food intake.

B_{12}-$PYY_{3–36}$ was shown to have a significantly (>10%) improved effect on inhibiting food intake in rats compared with $PYY_{3–36}$ when viewed over the 5-day course of treatment. Consistent with the sc $PYY_{3–36}$ administration work of Chelikani et al (36), the effects of both the conjugate and $PYY_{3–36}$ decrease after the 3- to 4-day mark, a result they ascribe to hyperphagia. When compared with $PYY_{3–36}$ over the first 3 days of the treatment period, B_{12}-$PYY_{3–36}$ resulted in an even stronger reduction of food intake (14.4% vs 30.1%, respectively; Figure 5B), although similar in body weight gain (Figure 7). On treatment days 4 and 5, stronger reductions in food intake continue for the B_{12}-$PYY_{3–36}$- vs $PYY_{3–36}$-treated rats (Figure 5B); however, our study did not show a significant reduction of body weight gain beyond 3 days of treatment (Figure 7). This shift back to normal body weight gain is consistent with the work of Pittner et al (37) and Chelikani et al (36). Despite a reduced efficacy, food intake remained significantly lower through the 10-day extended B_{12}-$PYY_{3–36}$ treatment as compared with baseline, indicating a continued effect (Figure 5, C and D). The reduced overall effect of treatment may be due to the development of rebound hyperphagia between infusions (Supplemental Figure 6). The inactive null control, B_{12}-PYY_{C36}, did not lead to a reduction of food intake (Figure 5, B and D) or body weight gain (Figure 7), documenting that B_{12} itself does not contribute to the observed effects on food intake. The use of a lean rat model may have hastened the activation of an orexigenic compensatory mechanism protecting animals from excessive weight loss, especially considering the dramatic reduction in food intake caused by the B_{12}-$PYY_{3–36}$ conjugate. Further studies will need to account for changes in activity and thermogenesis to elucidate the causes of the observed discrepancy between changes in food intake and body weight gain.

Interestingly, we found a strong reduction of food intake consistently after each pulse of B_{12}-$PYY_{3–36}$ across the dark cycle but not after $PYY_{3–36}$. Additionally, the percentage change in food intake after each of the three dark cycle treatment pulses (Figure 6D) is inversely related to the magnitude of food intake during that time at baseline (Figure 4A).Given the sc mode of administration and the postulated improvement in absorption for the B_{12} conjugate, it is probable that the greater levels of achieved conjugate and improved tissue distribution (as evidenced by V_D/F) is producing the consistent effects. This observation is supported by the fact that both $PYY_{3–36}$ and B_{12}-$PYY_{3–36}$ have the same time of nadir of pulse (Figure 6A) but differ in pulse duration, especially during the first two doses of the dark cycle (Figure 6B). The improved function and the uniform nature of effects throughout the testing cycle produced by conjugation of B_{12} are of note for pharmaceutical development of hormone-based therapies.

Our current findings show that systemic $PYY_{3–36}$ and B_{12}-$PYY_{3–36}$ induce a similar elevation in Fos expression in the caudal NTS. This is consistent with previous reports detailing the effects of systemic $PYY_{3–36}$ to elicit Fos in the NTS (5) and implicate a direct and/or indirect action of

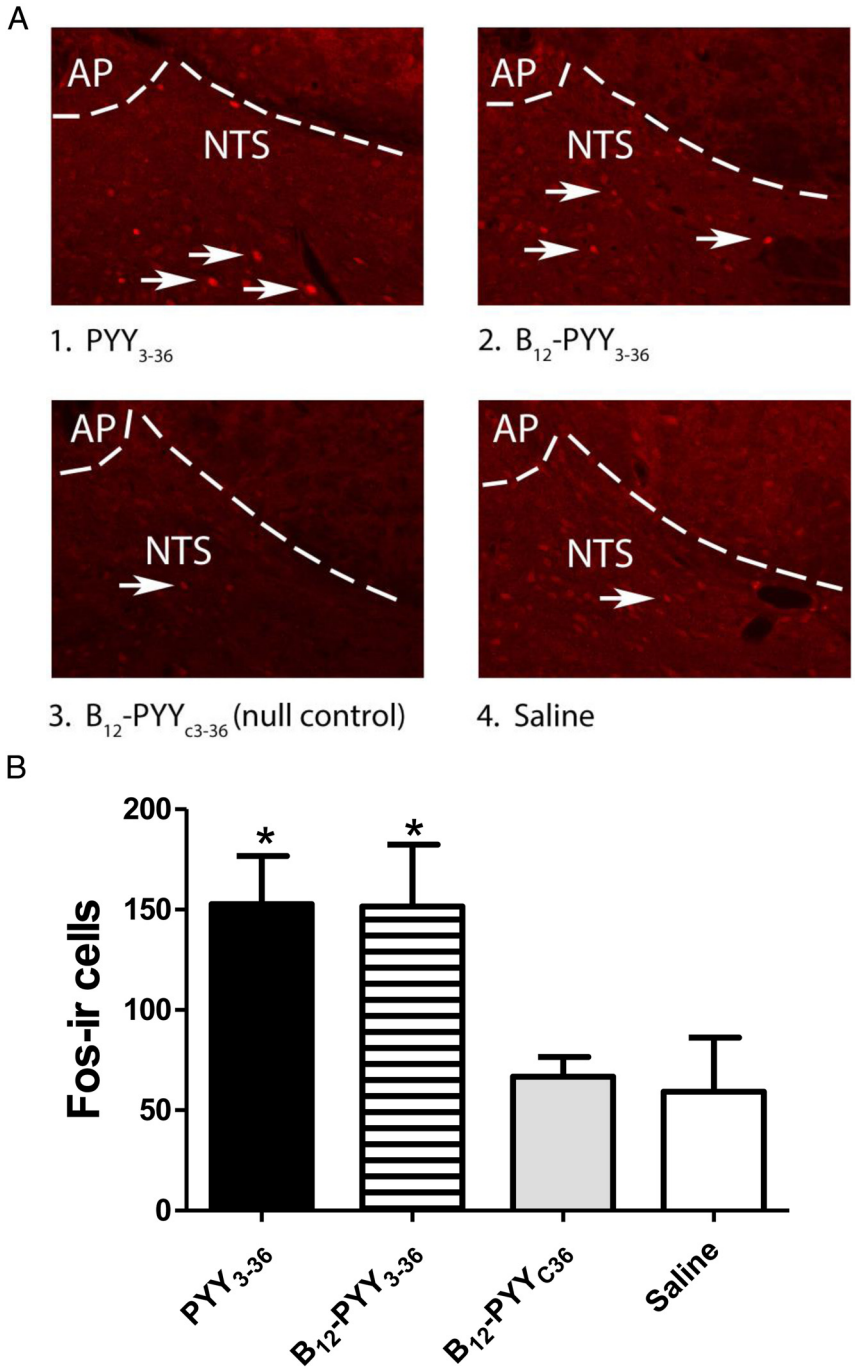

Figure 8. Effects of $PYY_{3–36}$ and B_{12}-$PYY_{3–36}$ on induction of Fos in the caudal NTS. Representative images showing immunofluorescent localization of Fos in nuclei of caudal NTS neurons activated by $PYY_{3–36}$ or B_{12}-$PYY_{3–36}$ (indicated by white arrows) (A). Fos (+) cells in coronal sections of rat hindbrain are shown in animals treated with $PYY_{3–36}$ (1), B_{12}-$PYY_{3–36}$ (2), B_{12}-PYY_{C36} (null control) (3), or saline (4) at the level of the AP and NTS (B). Panels 1–4 are all visualized at ×20 magnification (A). Mean number of Fos (+) nuclei across four anatomically matched levels of the caudal NTS after sc injection of $PYY_{3–36}$, B_{12}-$PYY_{3–36}$, B_{12}-PYY_{C36}, or saline are shown. *, $P < .05$ vs vehicle or B_{12}-PYY_{C36} (B).

both compounds on hindbrain neurons that integrate information pertaining to the regulation of food intake and control of meal size (38–40). $PYY_{3–36}$ is capable of penetrating the BBB (30) and activating vagal sensory nerves (4); however, it is not clear to what extent the effects of $PYY_{3–36}$ and B_{12}-$PYY_{3–36}$ occur through a direct action at NPY2 receptors expressed in the NTS (41, 42) or nodose ganglion (4) whose administration of a NPY2 receptor antagonist on projections terminate in the NTS (41–44). Further studies that examine the effectiveness of fourth ventricular the ability of systemic administration $PYY_{3–36}$ or B_{12}-$PYY_{3–36}$ to inhibit food intake and elicit Fos in the NTS will help elucidate a direct or indirect mechanism of action.

The in vivo uptake profile of $PYY_{3–36}$ and the B_{12}-$PYY_{3–36}$ conjugate was examined via ELISA over the course of a 5-hour time period. The B_{12}-$PYY_{3–36}$ conjugate showed a peak concentration of plasma $PYY_{3–36}$ at 2520 ± 257 pg/mL at approximately 1 hour after the sc injection at 10 nmol/kg. After the administration of free $PYY_{3–36}$ at the same dose, plasma $PYY_{3–36}$ concentration had the same trend but peaked at a lower concentration (C_{max} 1680 ± 243 pg/mL at 1 h). The AUC_{ext} for B_{12}-$PYY_{3–36}$ was greater (7130 ± 2050 pg/h/mL) than $PYY_{3–36}$ (3843 ± 1125 pg/h/mL). The improved half-life of the B_{12}-$PYY_{3–36}$ conjugate (half-life 1.34 ± 0.28 h) vs free $PYY_{3–36}$ (half-life 0.82 ± 0.16 h) is carried over from the decreased clearance rate for the conjugate and increased volume of distribution. Improved tissue distribution was also indicated by a higher volume of distribution for B_{12}-$PYY_{3–36}$, which may be in part due to the B_{12} uptake and the BBB transporter CD320 (the suggestion being function herein beyond vagal afferent communication). These preliminary hypotheses warrant further studies and more extensive pharmacokinetics with both the B_{12}-$PYY_{3–36}$ conjugate and free $PYY_{3–36}$.

There are several limitations to this study that need to be addressed in future experiments. First, Fos activation was only measured at one time point after the drug ad-

ministration; a dose response experiment will need to be performed to determine whether there is any difference in hindbrain Fos activation due to B_{12}-$PYY_{3–36}$ compared with $PYY_{3–36}$. In addition, it has been shown that systemic injections of albumin-$PYY_{3–36}$ has shown decreased food intake (23), suggesting a peripheral mechanism due to vagal-afferent signaling. Additional immunohistological studies will be performed to determine the presence of TCII, B_{12}, and $PYY_{3–36}$ in the brain to further elucidate whether Fos activation and/or reduction of food intake was due to a vagal-afferent mechanism or as a result of BBB crossing. Also, the presented study did not include any measures of energy expenditure, which could help explain the opposing changes in food intake and body weight gain that occurred after the third day of B_{12}-$PYY_{3–36}$ treatment. Additionally, the use of lean animals could have impacted the efficacy of the B_{12}-$PYY_{3–36}$ treatment with respect to long-term reductions of body weight gain, although the work of Pittner et al (37) demonstrated no loss of compensation via sc administration of $PYY_{3–36}$ after 3–4 days in either lean or obese rat models. Chelikani et al (45) and Reidelberger et al (46) also demonstrated intermittent ip injections of $PYY_{3–36}$ reduces daily food intake and body weight gain in obese rats. Future studies will include diet induced obese rats to assay for whether the B_{12} conjugate can overcome the compensation observed by Pittner et al (37) and continuous measures of activity and body temperature to better characterize the effects of B_{12}-$PYY_{3–36}$.

In summary, our study demonstrates that the reduction of daily food intake and weight gain were stronger for a conjugate of B_{12} and $PYY_{3–36}$ as compared with $PYY_{3–36}$ alone. More consistent and longer inhibition of food intake after pulses of B_{12}-$PYY_{3–36}$ conjugate vs native $PYY_{3–36}$ may be explained by greater sc absorption through conjugation of the gut hormone to B_{12}. Questions raised herein will be addressed in follow-up experiments, which will also test the anorectic effects of the B_{12}-$PYY_{3–36}$ upon oral delivery.

Acknowledgments

The authors acknowledge Dr Damian Allis (Syracuse University, Syracuse, New York) for the rendering of Figure 1B. We thank Dr Evi Kostenis (University of Bonn, Bonn, Germany) for providing the GαqG66Di5 plasmid used in the in vitro assays. We thank Dr Randall Sakai (Cincinnati, Ohio) for graciously providing us with the AccuScan DietMax cages as well as Benjamin W. Thompson and Nishi Ivanov, who provided technical assistance with brain processing and Fos assays. The authors also wish to thank Dr. David Griffith (Pfizer, Boston, MA) for helpful discussion on the pharmacokinetic analysis.

Address all correspondence and requests for reprints to: Robert P. Doyle, PhD, Department of Chemistry, Center for Science and Technology, Syracuse University, 111 College Place, Syracuse, NY 13244. Phone: 315-443-2925, E-mail: rpdoyle@syr.edu; or Christian L. Roth, MD, Division of Endocrinology, Center for Integrative Brain Research, Seattle Children's Research Institute, 1900 Ninth Avenue, Seattle, WA 98101. Phone: 206-987-5428, E-mail: christian.roth@seattlechildrens.org.

This work was supported by the National Institute of Diabetes and Digestive and Kidney Diseases/National Institutes of Health/Department of Health and Human Services Grant NIH-R15DK097675-01A1 (to R.P.D. and C.L.R.), the Arnold and Mabel Beckman Foundation (to R.P.D.), and by the Department of Veterans Affairs Merit Review Research Program (to J.E.B.). Additional support included the Research and Development Service of the Department of Veterans Affairs and the Cellular and Molecular Imaging Core of the Diabetes Research Center at the University of Washington and National Institutes of Health Grant P30DK017047.

Disclosure Summary: The authors have nothing to declare.

References

1. **Karra E, Batterham RL.** The role of gut hormones in the regulation of body weight and energy homeostasis. *Mol Cell Endocrinol*. 2010; 316(2):120–128.
2. **Batterham RL, Cowley MA, Small CJ, et al.** Gut hormone PYY3–36 physiologically inhibits food intake. *Nature* 2002;418(6898):650–654.
3. **Broom DR, Batterham RL, King JA, Stensel DJ.** Influence of resistance and aerobic exercise on hunger, circulating levels of acylated ghrelin, and peptide YY in healthy males. *Am J Physiol Regul Integr Comp Physiol*. 2009;296(1):R29–R35.
4. **Koda S, Date Y, Murakami N, et al.** The role of the vagal nerve in peripheral PYY3–36-induced feeding reduction in rats. *Endocrinology*. 2005;146(5):2369–2375.
5. **Blevins JE, Chelikani PK, Haver AC, Reidelberger RD.** PYY(3–36) induces Fos in the arcuate nucleus and in both catecholaminergic and non-catecholaminergic neurons in the nucleus tractus solitarius of rats. *Peptides*. 2008;29(1):112–119.
6. **Halatchev IG, Ellacott KL, Fan W, Cone RD.** Peptide YY3–36 inhibits food intake in mice through a melanocortin-4 receptor-independent mechanism. *Endocrinology*. 2004;145(6):2585–2590.
7. **Neary NM, Small CJ, Druce MR, et al.** Peptide YY3–36 and glucagon-like peptide-17–36 inhibit food intake additively. *Endocrinology*. 2005;146(12):5120–5127.
8. **Moran TH, Smedh U, Kinzig KP, Scott KA, Knipp S, Ladenheim EE.** Peptide YY(3–36) inhibits gastric emptying and produces acute reductions in food intake in rhesus monkeys. *Am J Physiol Regul Integr Comp Physiol*. 2005;288(2):R384–R388.
9. **Koegler FH, Enriori PJ, Billes SK, et al.** Peptide YY(3–36) inhibits morning, but not evening, food intake and increases body weight in rhesus macques. *Diabetes* 2005;54(11):3198–3204.
10. **Helou N, Obeid O, Azar ST, Hwalla N.** Variation of postprandial PYY 3–36 response following ingestion of differing macronutrient meals in obese females. *Ann Nutr Metab*. 2008;52(3):188–195.
11. **Batterham RL, Cowley MA, Ellis SM, et al.** Inhibition of food intake in obese subjects by peptide YY3–36. *N Engl J Med*. 2003;349(10): 941–948.
12. **Abbott CR, Monteiro M, Small CJ, et al.** The inhibitory effects of peripheral administration of peptide YY(3–36) and glucagon-like

peptide-1 on food intake are attenuated by ablation of the vagal-brainstem-hypothalamic Pathway. *Brain Res*. 2005;1044(1):127–131.
13. **Chelikani PK, Haver AC, Reidelberger RD.** Comparison of the inhibitory effects of PYY(3–36) and PYY(1–36) on gastric emptying in rats. *Am J Physiol Regul Integr Comp Physiol*. 2004;287(5):R1064–R1070.
14. **le Roux CW, Batterham RL, Aylwin SJ, et al.** Attenuated peptide YY release in obese subjects is associated with reduced satiety. *Endocrinology*. 2006;147(1):3–8.
15. **Roth CL, Bongiovanni KD, Gohlke B, Woelfle J.** Changes in dynamic insulin and gastrointestinal hormone secretion in obese children. *J Pediatr Endocrinol Metab*. 2010;23(12):1299–1309.
16. **Roth CL, Enriori PJ, Harz K, Woelfle J, Cowley MA, Reinehr T.** Peptide YY is a regulator of energy homeostasis in obese children before and after weight loss. *J Clin Endocrinol Metab*. 2005;90(12):6386–6391.
17. **Addison ML, Minnion JS, Shillito JC, et al.** A role for metalloendopeptidases in the breakdown of the gut hormone, PYY 3–36. *Endocrinology*. 2011;152(12):4630–4640.
18. **Gantz I, Erondu N, Mallick M, et al.** Efficacy and safety of intranasal peptide YY3–36 for weight reduction in obese adults. *J Clin Endocrinol Metab*. 2007;92(5):1754–1757.
19. **Halatchev IG, Cone RD.** Peripheral administration of PYY(3–36) produces conditioned taste aversion in mice. *Cell Metab*. 2005;1(3):159–168.
20. **Degen L, Oesch S, Casanova M, et al.** Effect of peptide YY3–36 on food intake in humans. *Gastroenterology*. 2005;129(5):1430–1436.
21. **Shechter Y, Tsubery H, Mironchik M, Rubinstein M, Fridkin M.** Reversible PEGylation of peptide YY3–36 prolongs its inhibition of food intake in mice. *FEBS Lett*. 2005;579(11):2439–2444.
22. **Ehrlich GK, Michel H, Truitt T, et al.** Preparation and characterization of albumin conjugates of a truncated peptide YY analogue for half-life extension. *Bioconjug Chem*. 2013;24(12):2015–2024.
23. **Baraboi ED, Michel C, Smith P, Thibaudeau K, Ferguson AV, Richard D.** Effects of albumin-conjugated PYY on food intake: the respective roles of the circumventricular organs and vagus nerve. *Eur J Neurosci*. 2010;32(5):826–839.
24. **Nielsen MJ, Rasmussen MR, Andersen CB, Nexo E, Moestrup SK.** Vitamin B12 transport from food to the body's cells—a sophisticated, multistep pathway. *Nat Rev Gastroenterol, Hepatol*. 2012;9(6):345–354.
25. **Russell-Jones GJ, Westwood S, Farnworth PG, Findlay JK, Burger HG.** Synthesis of LHRH antagonists suitable for oral administration via the vitamin B12 uptake system. *Bioconjug Chem*. 1995;6(1)34–42.
26. **Russell-Jones GJ, Westwood S, Habberfield AD.** Vitamin B12 mediated oral delivery systems for granulocyte-colony stimulating factor and erythropoietin. *Bioconjug Chem*. 1995;6(1):459–465.
27. **Petrus AK, Vortherms AR, Fairchild TJ, Doyle RP.** Vitamin B12 as a carrier for the oral delivery of insulin. *ChemMedChem*. 2007;2(12):1717–1721.
28. **Fazen CH, Valentin D, Fairchild TJ, Doyle RP.** Oral delivery of the appetite suppressing peptide hPYY(3–36) through the vitamin B12 uptake pathway. *J Med Chem*. 2011;54(24):8707–8711.
29. **Clardy-James S, Chepurny OG, Leech CA, Holz GG, Doyle RP.** Synthesis, characterization and pharmacodynamics of vitamin-B(12)-conjugated glucagon-like peptide-1. *ChemMedChem*. 2013;8(4):582–586.
30. **Nonaka N, Shioda S, Niehoff ML, Banks WA.** Characterization of blood-brain barrier permeability to PYY3–36 in the mouse. *J Pharmacol Exp Ther*. 2003;306(3):948–953.
31. **Lazar GS, Carmel R.** Cobalamin binding and uptake in vitro in the human central nervous system. *J Lab Clin Med*. 1981;97(1):123–133.
32. **Kostenis E, Martini L, Ellis J, et al.** A highly conserved glycine within linker I and the extreme C terminus of G protein α subunits interact cooperatively in switching G protein-coupled receptor-to-effector specificity. *J Pharmacol Exp Ther*. 2005;313(1):78–87.
33. **Pedersen SL, Holst B, Vrang N, Jensen KJ.** Modifying the conserved C-terminal tyrosine of the peptide hormone PYY3–36 to improve Y2 receptor selectivity. *J Pept Sci*. 2009;15(11):753–759.
34. **Kolb HC, Finn MG, Sharpless, KB.** Click chemistry: diverse chemical function from a few good reactions. *Angew Chem Int Ed*. 2001;40(11):2004–2021.
35. **Vrang N, Madsen AN, Tang-Christensen M, Hansen G, Larsen PJ.** PYY(3–36) reduces food intake and body weight and improves insulin sensitivity in rodent models of diet-induced obesity. *Am J Physiol Regul Integr Comp Physiol*. 2006;291(2):R367–R375.
36. **Chelikani PK, Haver AC, Reeve JR, Keire DA, Reidelberger RD.** Daily, intermittent intravenous infusion of peptide YY(3–36) reduces daily food intake and adiposity in rats. *Am J Physiol Regul Integr Comp Physiol*. 2006;290(2):R298–R305.
37. **Pittner RA, Moore CX, Bhavsar SP, et al.** Effects of PYY[3–36] in rodent models of diabetes and obesity. *In J Obes Relat Metab Disord*. 2004;28(8):963–971.
38. **Chen DY, Deutsch JA, Gonzalez MF, Gu Y.** The induction and suppression of c-fos expression in the rat brain by cholecystokinin and its antagonist L364,718. *Neurosci Lett*. 1993;149(1):91–94.
39. **Day HE, McKnight AT, Poat JA, Hughes J.** Evidence that cholecystokinin induces immediate early gene expression in the brainstem, hypothalamus and amygdala of the rat by a CCKA receptor mechanism. *Neuropharmacology*. 1994;33(6):719–727.
40. **Fraser KA, Raizada E, Davison JS.** Oral-pharyngeal-esophageal and gastric cues contribute to meal-induced c-fos expression. *Am J Physiol*. 1995;268(1 Pt 2):R223–R230.
41. **Parker RM, Herzog H.** Regional distribution of Y-receptor subtype mRNAs in rat brain. *Eur J Neurosci*. 1999;11(4):1431–1448.
42. **Mahaut S, Dumont Y, Fournier A, Quirion R, Moyse E.** Neuropeptide Y receptor subtypes in the dorsal vagal complex under acute feeding adaptation in the adult rat. *Neuropeptides*. 2010;44(2):77–86.
43. **Shapiro RE, Miselis RR.** The central organization of the vagus nerve innervating the stomach of the rat. *J Comp Neurol*. 1985;238(4):473–488.
44. **Kalia M, Mesulam MM.** Brain stem projections of sensory and motor components of the vagus complex in the cat: I. The cervical vagus and nodose ganglion. *J Comp Neurol*. 1980;193(2):435–465.
45. **Chelikani PK, Haver AC, Reidelberger RD.** Intermittent intraperitoneal infusion of peptide YY(3–36) reduces daily food intake and adiposity in obese rats. *Am J Physiol Regul Integr Comp Physiol*. 2007;293(1):R39–R46.
46. **Reidelberger RD, Haver AC, Chelikani PK, Buescher JL.** Effects of different intermittent peptide YY (3–36) dosing strategies on food intake, body weight, and adiposity in diet-induced obese rats. *Am J Physiol Regul Integr Comp Physiol*. 2008;295(2):R449–R458.

All chemicals, reagents, and solvents were purchased from Sigma-Aldrich, Alfa Aesar, J.T. Baker, VWR, or Thermo Fisher Scientific (USA) and used without further purification. An Agilent 1200 reverse-phase high-performance liquid chromatography (HPLC) instrument with a manual injector and automated fraction collector was used for all HPLC purifications. An Eclipse XBD C_{18} analytical column (5 μm, 4.6 x 150 mm, Agilent) was used in all purifications. All mass spectra were obtained using a Bruker Autoflex III Matrix-Assisted Laser Desorption/Ionization Time of Flight Mass Spectrometer (MALDI-ToF MS). Peptide and protein concentrations were determined via Bradford Assay using a BIO-RAD Bovine Serum Albumin (BSA) standard (2 $mg \cdot mL^{-1}$). PYY_{3-36} with a K4 modified to azide and PYY_{C36} were ordered from C.S. Bio Corporation (Cambridge, MA). A Flex Station 3 Microplate Reader was used for all fluorescence-based plate assays. All plasmids were isolated using a mini plasmid isolation kit (VWR). F12-K (Kaighn's modification of Ham's F-12 medium) was purchased from the American Type Culture Collection. Trypsin/EDTA cocktail, fetal bovine serum (FBS), and Penicillin/Streptomycin cocktail (PenStrep) were ordered from Life Technologies.

Overview of Synthesis, purification, and characterization of B_{12}-PYY_{3-36} and B_{12}-PYY_{C36} conjugates

B_{12}-AB was isolated in ~50% yield and > 95% purity via RP-HPLC (Figure S1A), confirmed by MALDI-ToF MS (Figure S1B) and fully characterized by NMR (Figure S2). B_{12}-spdp was isolated by RP-HPLC and confirmed via MALDI-ToF MS prior to conjugation to PYY_{C36}. B_{12}-PYY_{3-36} (~25% isolated yield) and B_{12}-PYY_{C36} (~30% isolated yield) were purified to > 98% purity via RP-HPLC (Figures S3A and S4A, respectively). B_{12}-PYY_{3-36} and B_{12}-PYY_{C36} were both confirmed via MALDI-ToF MS (Figures S3B and S4B, respectively).

Synthesis, Purification, and Characterization of B_{12}-amino butyne (B_{12}-AB)

B_{12}-carboxylic acid (1) (24 mg, 0.0175 mmol) was activated with 1-ethyl-3-(3-dimethylaminopropyl)carbodiimide (EDC, 33.6 mg, 0.175 mmol) and hydroxybenzotriazole (HOBt, 47.4 mg, 0.351 mmol) in anhydrous dimethyl sulfoxide (DMSO, 3 mL) under argon for 30 minutes. To this

activated mixture, 1-amino-3-butyne (12.11 mg, 0.175 mmol) was added and let stir overnight under argon. The reaction was precipitated with a 3:1 mixture of diethyl ether/acetone and centrifuged at 4,000*g* for 10 minutes. The pellet was dissolved in ddH_2O for purification via RP-HPLC. The crude reaction was purified using gradient of 10% acetonitrile (MeCN) and 90% 0.1% TFA in H_2O to 27% MeCN over 17 minutes, increased to 50% MeCN over 2.5 minutes, and decreased to 10% MeCN, 90% 0.1% TFA in H_2O over 2.5 minutes with UV detection at 360 nm, and a flow rate of 1.0 mL/min. The isolated compound was analyzed via MALDI-ToF MS with a 1:1 sample:matrix ratio using an α-cyano-4-hydroxycinnamic acid (CHCA) matrix and fully characterized via NMR.

Synthesis, Characterization, and Purification of B_{12}-PYY_{3-36}

CuI (0.6 mg, 2.45 μmol and TBTA (1.2 mg, 6.13 μmol) were mixed in argon-degassed DMF/H_2O (1:1, 2 mL) for 10 min at RT. PYY_{3-36} K4-azide (1 mg, 0.245 μmol) and B_{12}-AB (1.04 mg, 0.732 μmol) were added to the mixture and stirred for 24 h. The crude reaction was centrifuged at 4000*g* for 5 minutes to remove the catalyst and TBTA. B_{12}-PYY_{3-36} was purified via RP-HPLC using a gradient of 10% 0.1% TFA in MeCN, 90% 0.1% TFA in H_2O, increased to 40% 0.1% TFA in MeCN over 30 minutes. B_{12}-PYY_{3-36} was characterized via MALDI-ToF MS using a CHCA matrix plated in a 1:1 sample:matrix ratio.

Synthesis, purification, and characterization of B_{12}-spdp

B_{12}-ethylenediamine (2) (3 mg, 2.08 μmol), was dissolved in 1 mL 100 mM sodium phosphate buffer (pH 8) with 1 mM EDTA. To the solution, 25 μL of 25 mM of *N*-succinimidyl 3-(2-pyridyldithio)-propionate (SPDP) was added and reaction was stirred for 1 h. The B_{12}-spdp product was isolated via RP-HPLC using a gradient of 11% MeCN, 89% buffer 0.1% TFA in H_2O to 29% B over 18 minutes. The product was confirmed via MALDI-ToF MS using a CHCA matrix plated in a 1:1 sample:matrix ratio.

Synthesis, Purification, and Characterization of B_{12}-PYY_{C36}

PYY_{C36} (5 mg, 1.24 µmol) was dissolved in 1 mL 100 mM sodium phosphate buffer pH 8 with 1 mM EDTA. Isolated B_{12}-spdp (2 mg, 1.24 µmol) was added to the PYY_{C36} solution and reaction proceeded for 16 h at RT. B_{12}-PYY_{C36} was purified on a RP-HPLC using a gradient of 11% MeCN, 89% 0.1% TFA in H_2O to 40% B over 29 minutes. The product was confirmed via MALDI-ToF MS using a CHCA matrix plated in a 1:1 sample:matrix ratio.

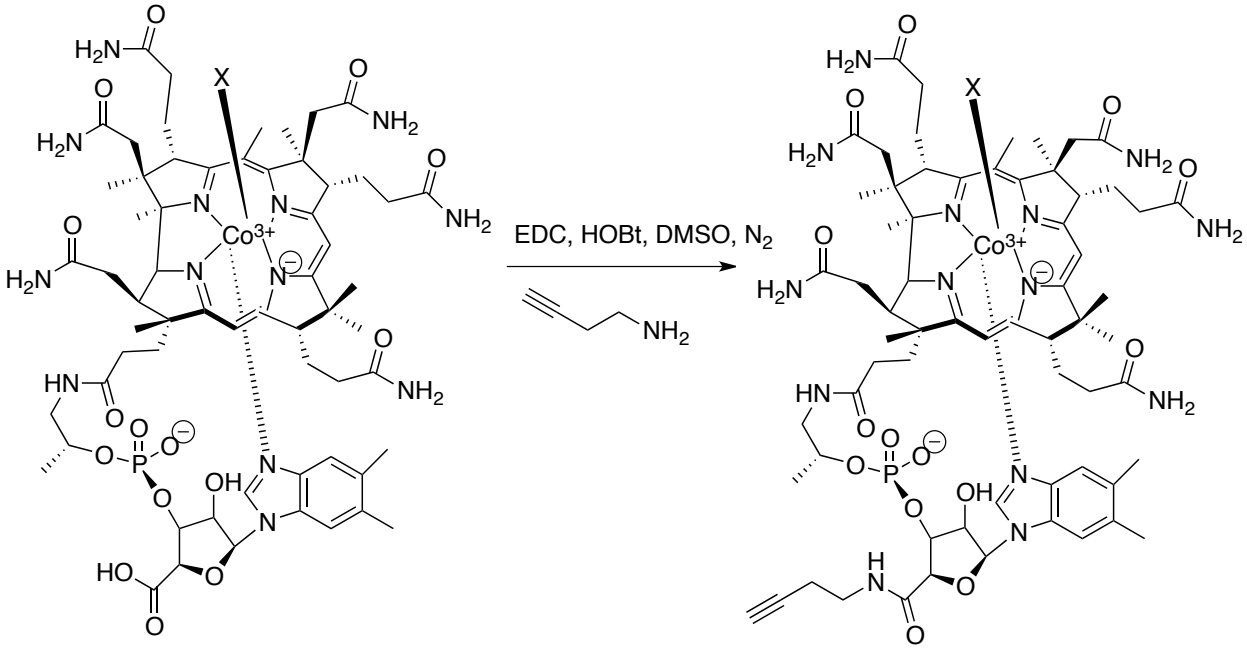

Scheme S1. Activation of B_{12}-CA with EDC/HOBt followed by addition of 1-amino-3-butyne under anhydrous conditions will result in formation of B_{12}-AB.

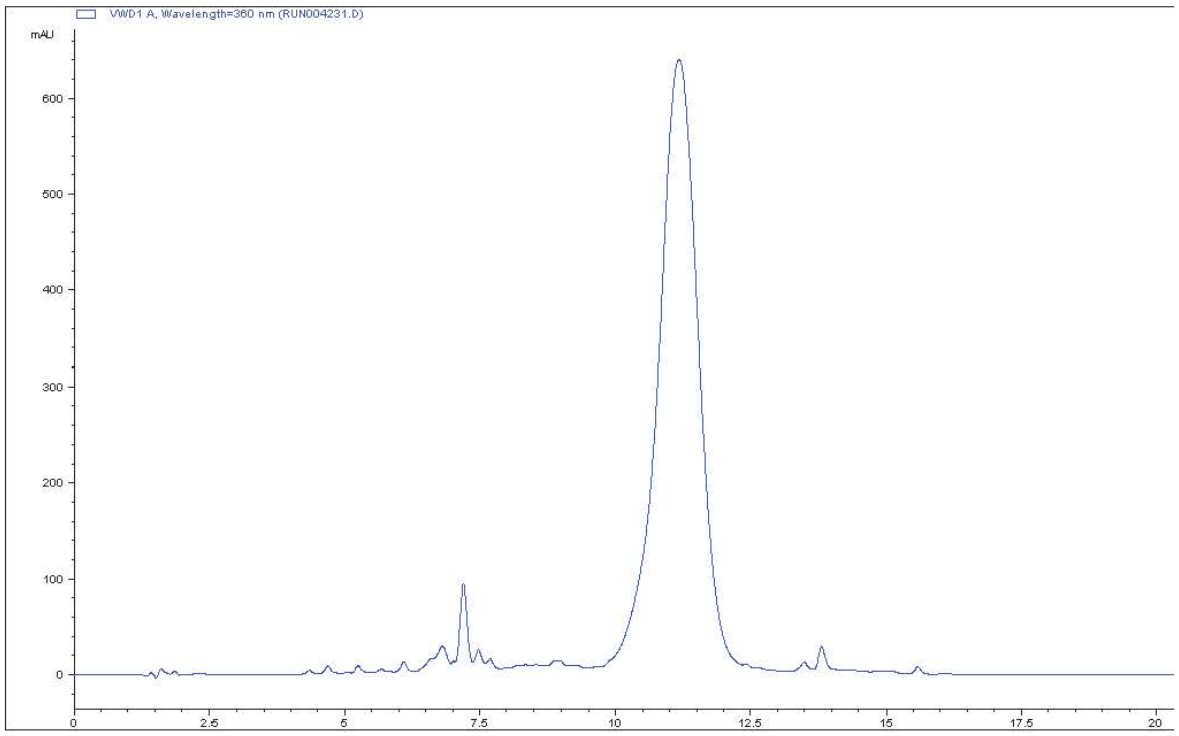

A

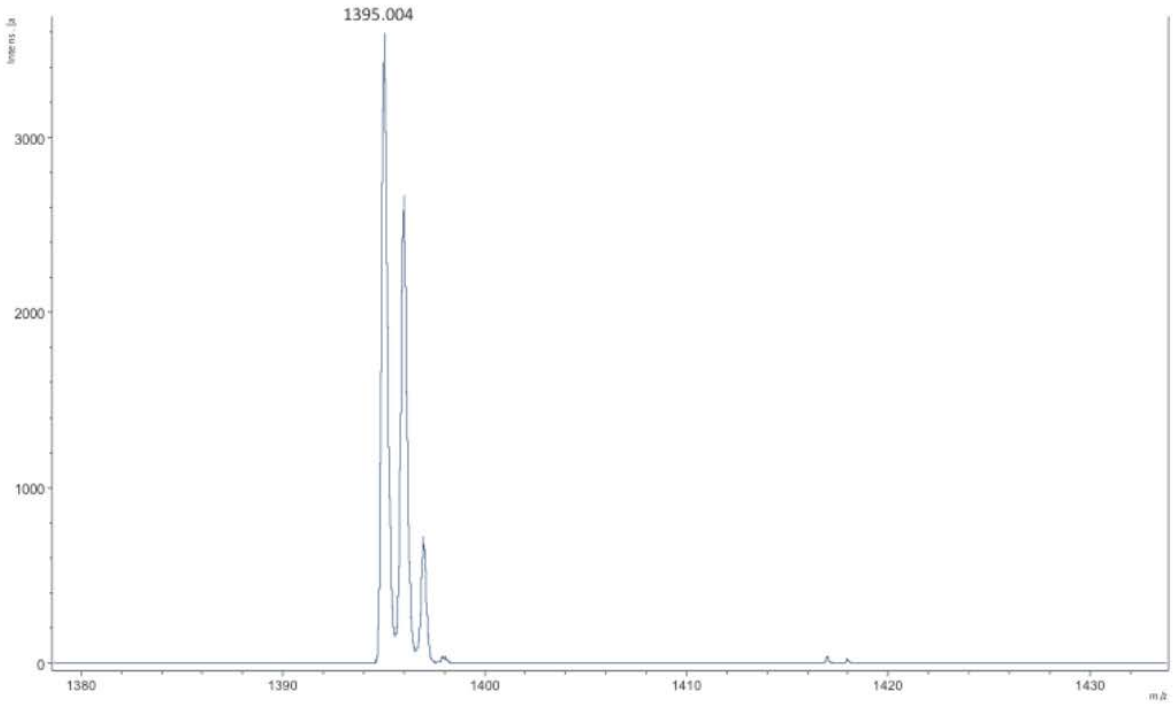

B

Figure S1. RP-HPLC trace of B_{12}-AB at 360 nm (A). Peak at t_R 11.2 min represents > 95% pure B_{12}-AB. MALDI-ToF MS of B_{12}-AB (B). Highlighted peak shows [M-CN] = 1395.

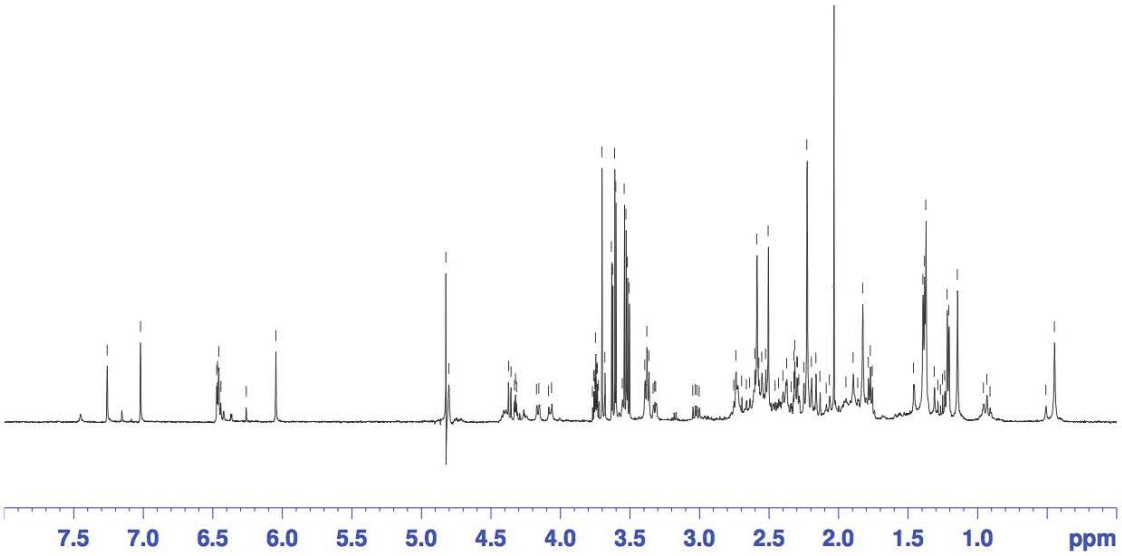

123 **A**

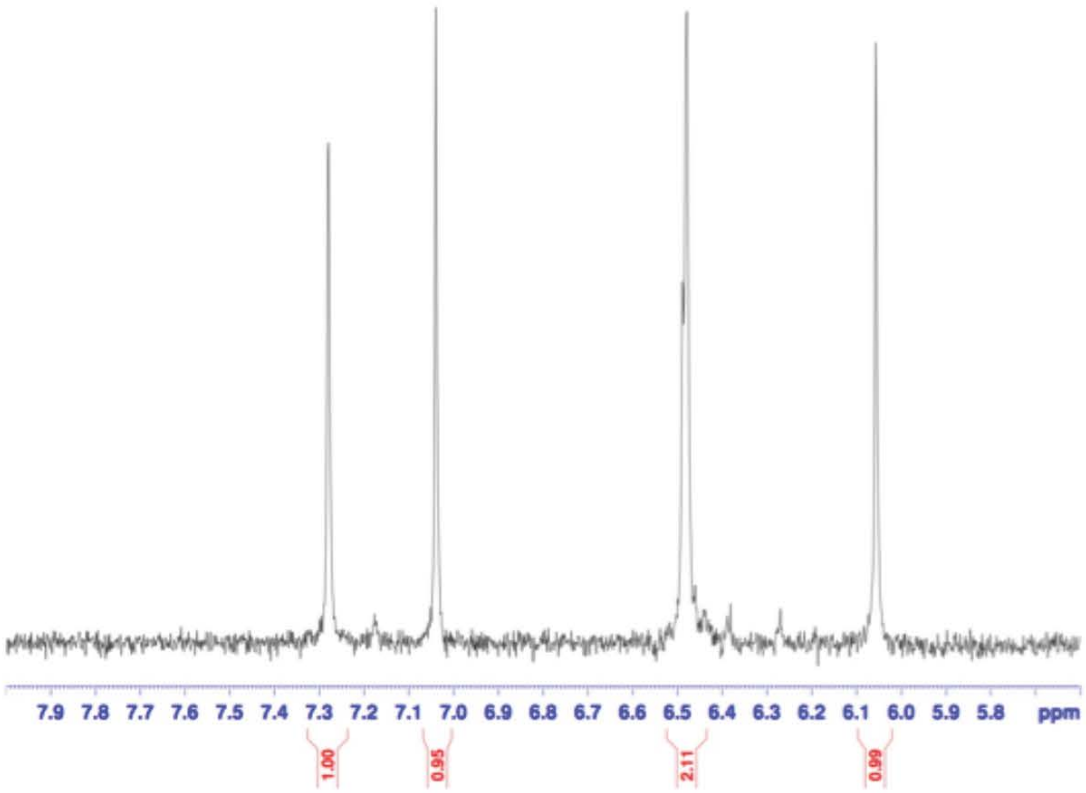

124 **B**

125 **Figure S2**. ^{1}H-NMR of B_{12}-AB in D_2O (A) with highlighted region of characteristic B_{12} protons in ^{1}H-

126 NMR of B_{12}-AB in D_2O on a 500 MHz spectrometer (B).

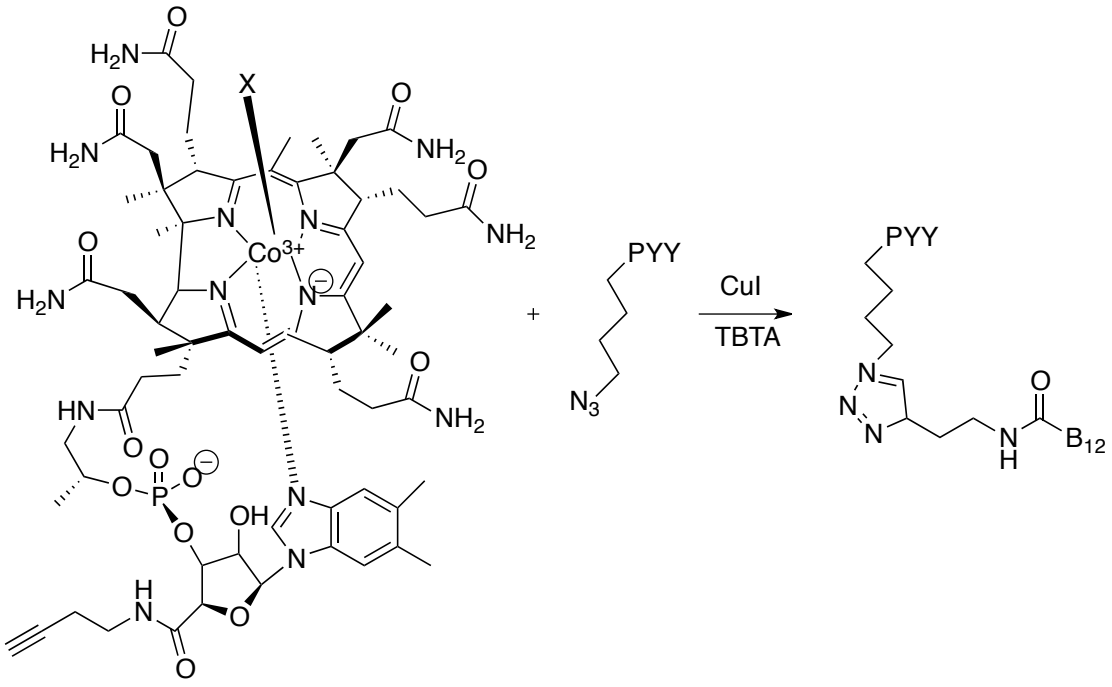

Scheme S2. Synthesis of B_{12}-PYY_{3-36} via Cu(I)-catalyzed cycloaddition with B_{12}-AB and modified PYY-K4 azide as starting material.

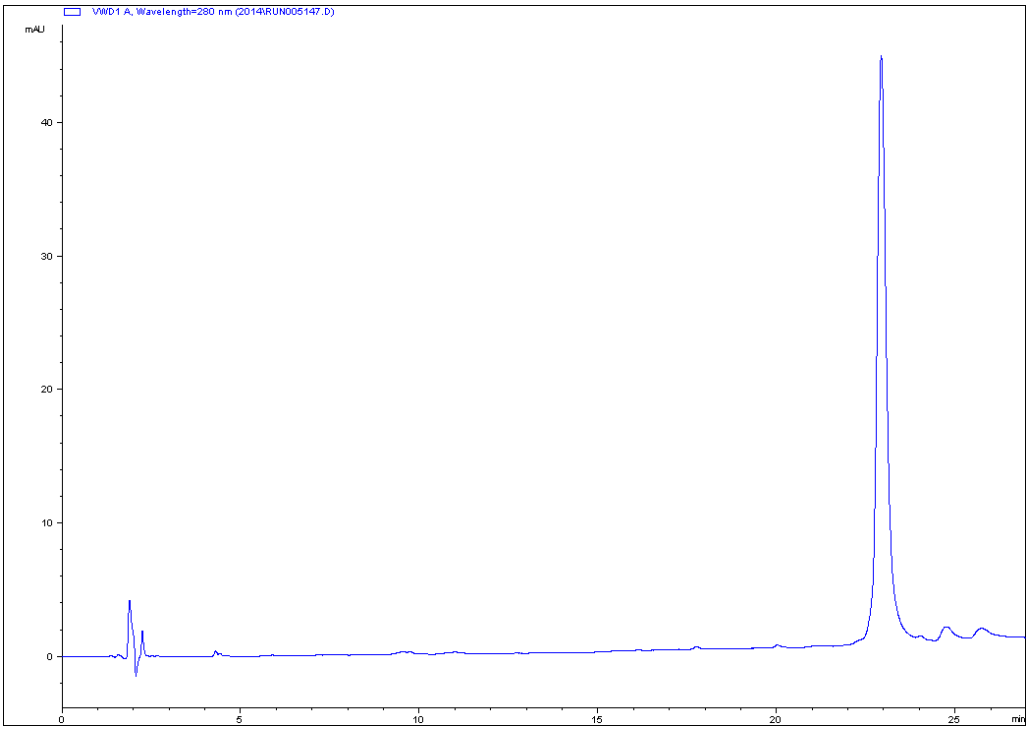

A

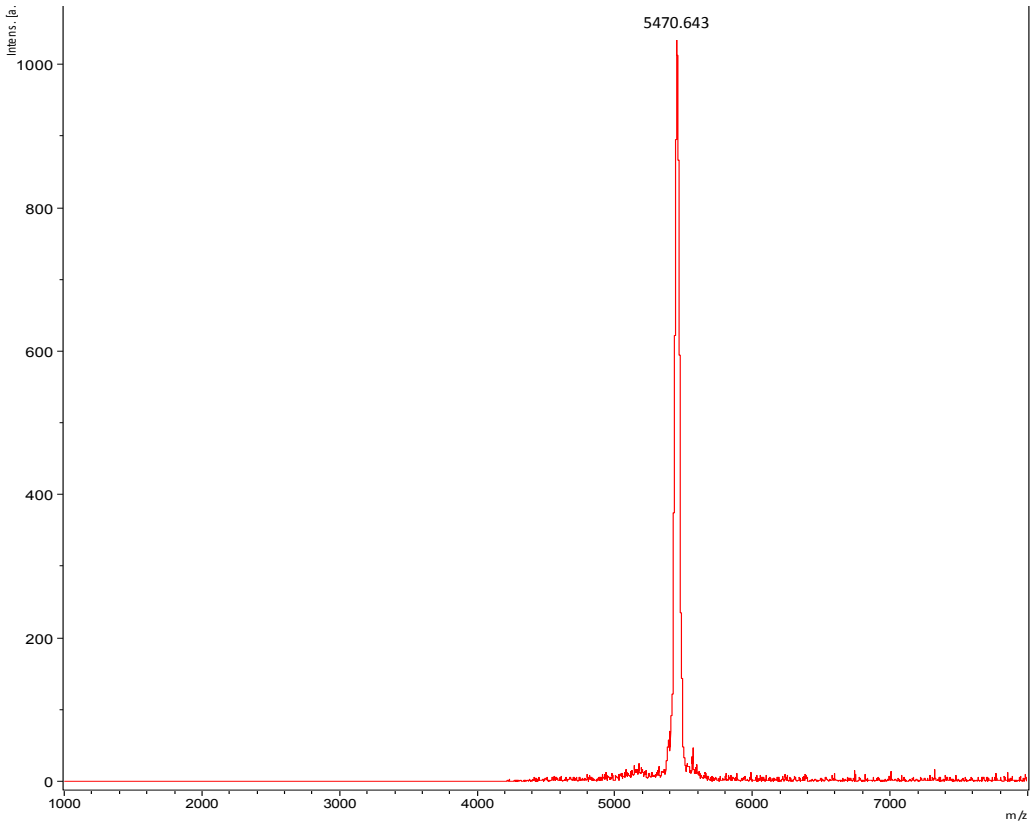

B

Figure S3. RP-HPLC of B_{12}-PYY_{3-36} at 280 nm. Peak at t_R = 23 min is desired product at > 98% purity (A). MALDI-ToF MS of B_{12}-PYY_{3-36} (B). Highlighted peak shows [M-CN] = 5470 m/z.

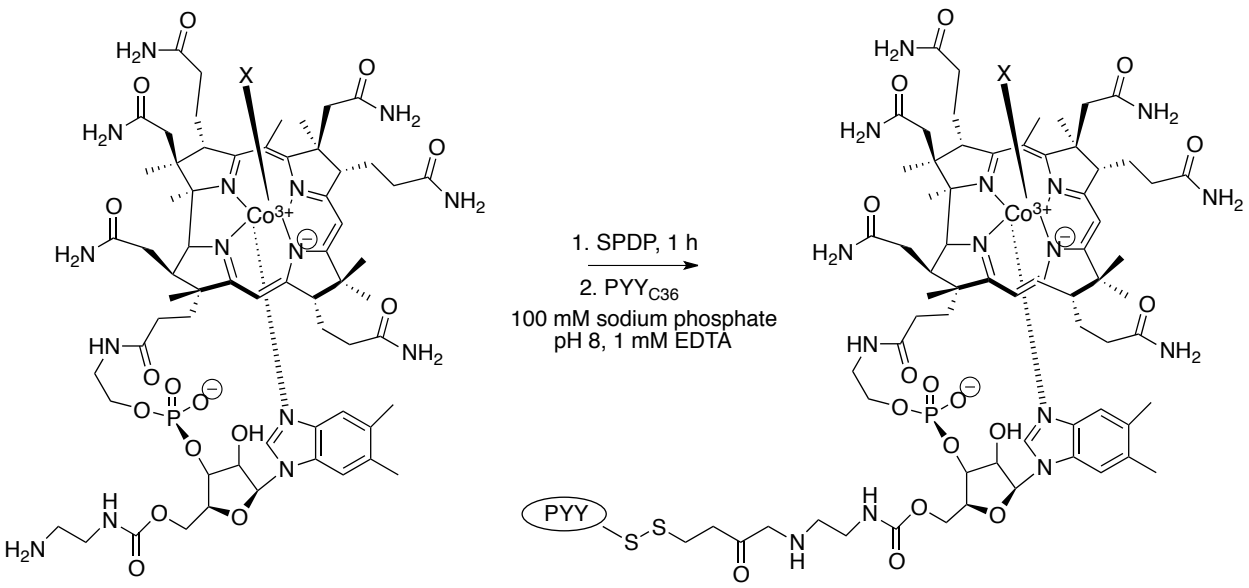

Scheme S3. Synthesis of B_{12}-PYY_{C36} via an SPDP linker and B_{12}-en precursor.

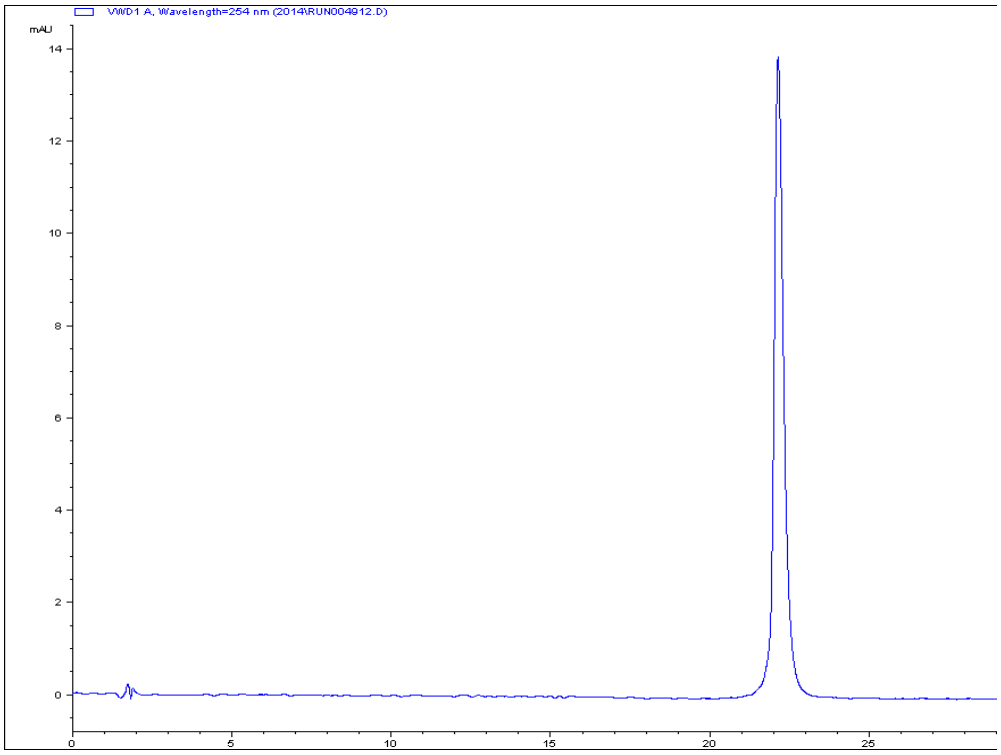

A

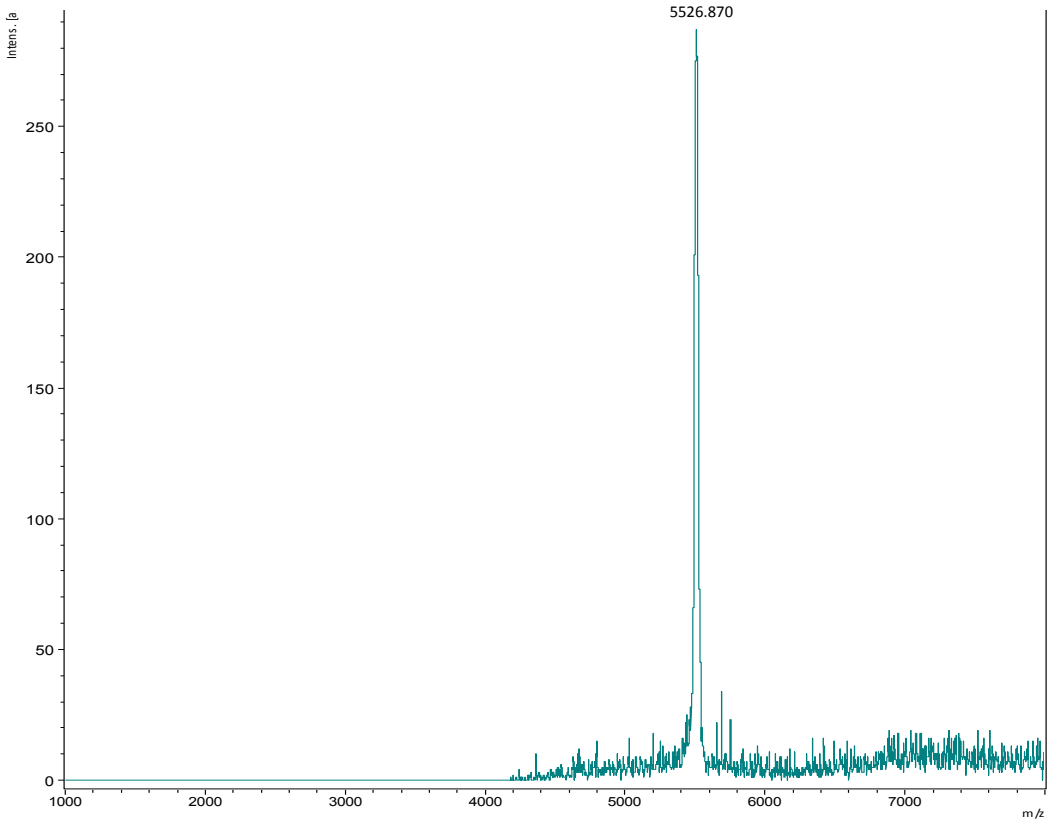

B

Figure S4. RP-HPLC purification of B_{12}-PYY_{C36} at 254 nm (A). Peak at t_R = 22.5 min is desired product.

MALDI-ToF MS of B_{12}-PYY_{C36} (B). Expected peak shown as [M-CN] = 5527 m/z.

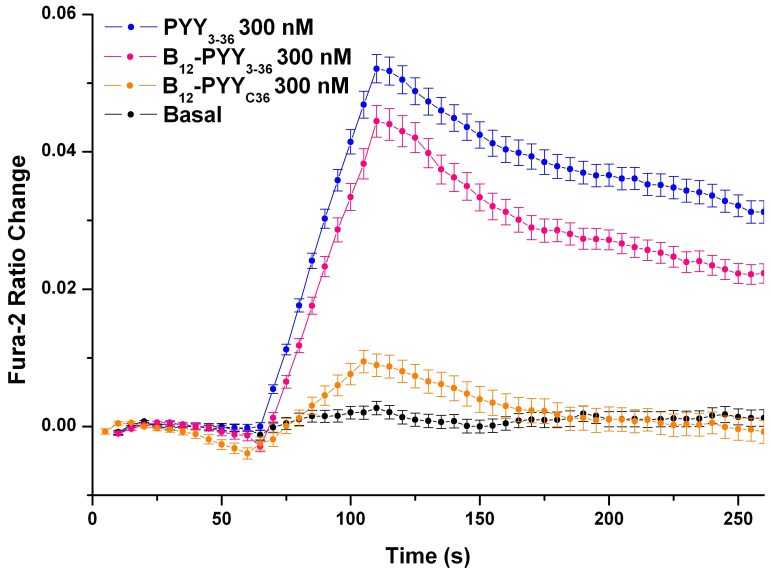

A

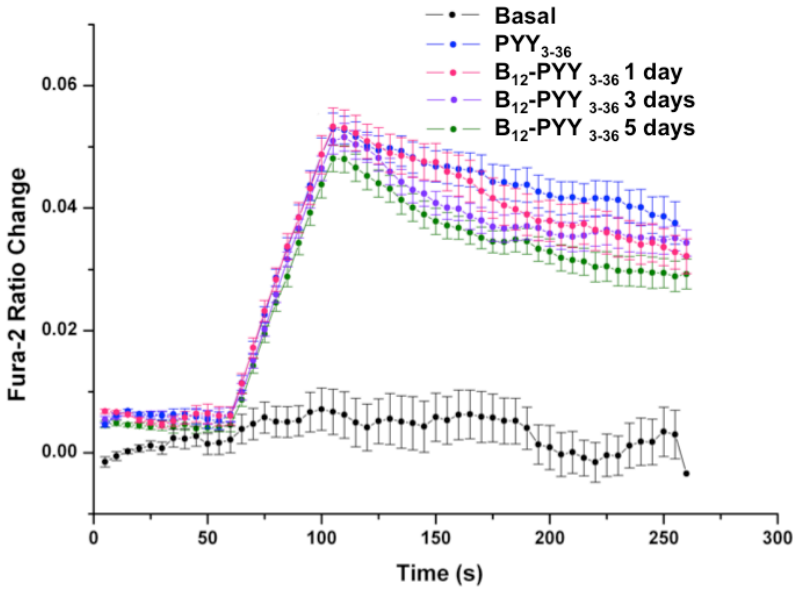

B

Figure S5. Activity profile of B_{12}-PYY_{3-36} and PYY_{3-36} vs. null control B_{12}-PYY_{C36} at 300 nM shows a drastic decrease in activity at the NPY2 receptor (A). Activity profile of B_{12}-PYY_{3-36} (all samples ran at 300 nM) when reconstituted in water and incubated at 37 °C for 1, 3, and 5 days in preparation for *in vivo* studies shows a minimal loss in activity (B).

Investigating the effect of subcutaneously administered B_{12}-PYY_{3-36} and B_{12}-PYY_{C36} in Fos activation in the hindbrain relative to PYY_{3-36} and saline.

Immunohistochemistry with antisera to c-Fos was performed on anatomically matched sections throughout the nucleus of the solitary tract (NTS) with tissue from every treatment condition included in every batch. Briefly, slides were washed 3 x 5 minutes at room temperature with 0.1 M PBS, then incubated in 5% normal goat serum in 1% BSA/0.1 M PBS for 30 minutes. Slides were incubated for 18-20 h at 4 °C with the primary antibody diluted in 1% BSA/0.1 M PBS solution. The primary antibody was a rabbit polyclonal anti-c-Fos (Table S1). This is a well-characterized antibody, which has been shown to be specific for its target molecule in previous studies (3, 4) and it stained the appropriate cellular and neuronal targets in our studies. Slides were rinsed 6 x 5 minutes in 0.1 M PBS and incubated with the secondary antibody for 60 minutes at room temperature. The secondary antibody was diluted in 1% BSA/0.1 M PBS. Slides were rinsed 6 x 5 minutes immediately prior to cover slipping using glycerol based mounting media. Staining specificity with the primary antibody was assessed by substituting rabbit serum (for anti-c-Fos antibody) at the same concentration used for the primary antibody and confirming the absence of staining. The specificity of the secondary antibody for the appropriate primary antibody IgG was verified in the dual staining protocol. Images of stained preparations were captured as jpeg files and converted to 8-bit jpeg files using a 20x objective and a COOLSNAPHQ2 Monochrome camera (Photometrics) attached to a Nikon Eclipse 80i fluorescent microscope (Nikon Instruments) and employing Nikon NIS-Elements Software. All saved images were adjusted for equal background brightness in Adobe Photoshop CS5 (Adobe Systems). Stained cells were counted manually by a single experimenter blind to treatment conditions. Bilateral counts were taken for cells expressing Fos across four coronal sections of the NTS at four different levels, each separated by approximately 280 μm. These levels corresponded to bregma -13.08 mm, -13.32 mm, -13.80 mm, and -14.04 mm, based on the rat brain atlas by Paxinos and Watson (5).

Table S1. Antibodies Utilized in Immunohistological Studies (abbreviations: C, centigrade; Gt, goat; IgG, immunoglobulin G; h, hours; Poly, polyclonal; Rb, rabbit; RT, room temperature).

Peptide/ Protein Target	Name of antibody	Manufacturer/ Catalog #	Host	Type	Titer	Incubation h, °C
c-Fos	anti-c-Fos	EMD Millipore; PC38T	Rb	Poly IgG	1:5000	18-20, 4
Rb IgG	Cy3 conjugated IgG (H+L)	Jackson ImmunoResearch Laboratories	Gt	Poly IgG	1:200	0.5, RT

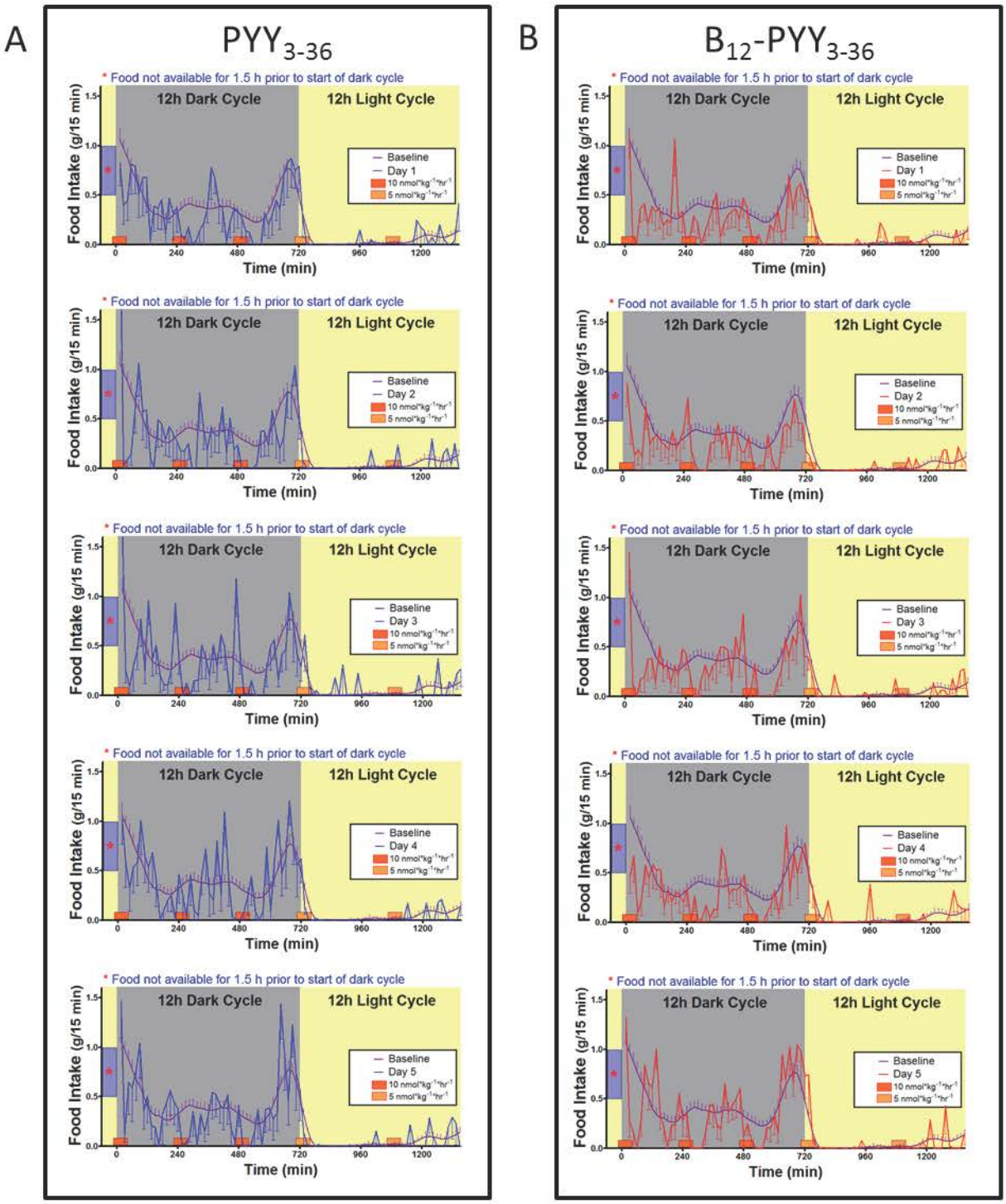

Figure S6. Feeding patterns during 5-day treatment with PYY_{3-36} (n = 8) (A) or B_{12}-PYY_{3-36} conjugate (n = 9) (B) averaged by day.

References

1. Clardy-James S, Bernstein JL, Kerwood DJ, and Doyle RP. Site-Selective Oxidation of Vitamin B_{12} Using 2-Iodoxybenzoic Acid. *Syn Lett.* 2012;23(16):2363-6.
2. Ikotun OF, Marquez BV, Fazen CH, Kahkoska AR, Doyle RP, and Lapi SE. Investigation of a vitamin B12 conjugate as a PET imaging probe. *ChemMedChem.* 2014;9(6):1244-51.
3. Blevins JE, Chelikani PK, Haver AC, and Reidelberger RD. PYY(3-36) induces Fos in the arcuate nucleus and in both catecholaminergic and non-catecholaminergic neurons in the nucleus tractus solitarius of rats. *Peptides* 2008;29(1):112-9.
4. Ho JM, Anekonda VT, Thompson BW, Zhu M, Curry RW, Hwang BH, Morton GJ, Schwartz MW, Baskin DG, Appleyard SM, et al. Hindbrain oxytocin receptors contribute to the effects of circulating oxytocin on food intake in male rats. *Endocrinology* 2014;155(8):2845-57.
5. Paxinos G.; Watson C. The rat brian stereotaxic coordinates. *Burlington: Academic Press.* 2007;6th ed.